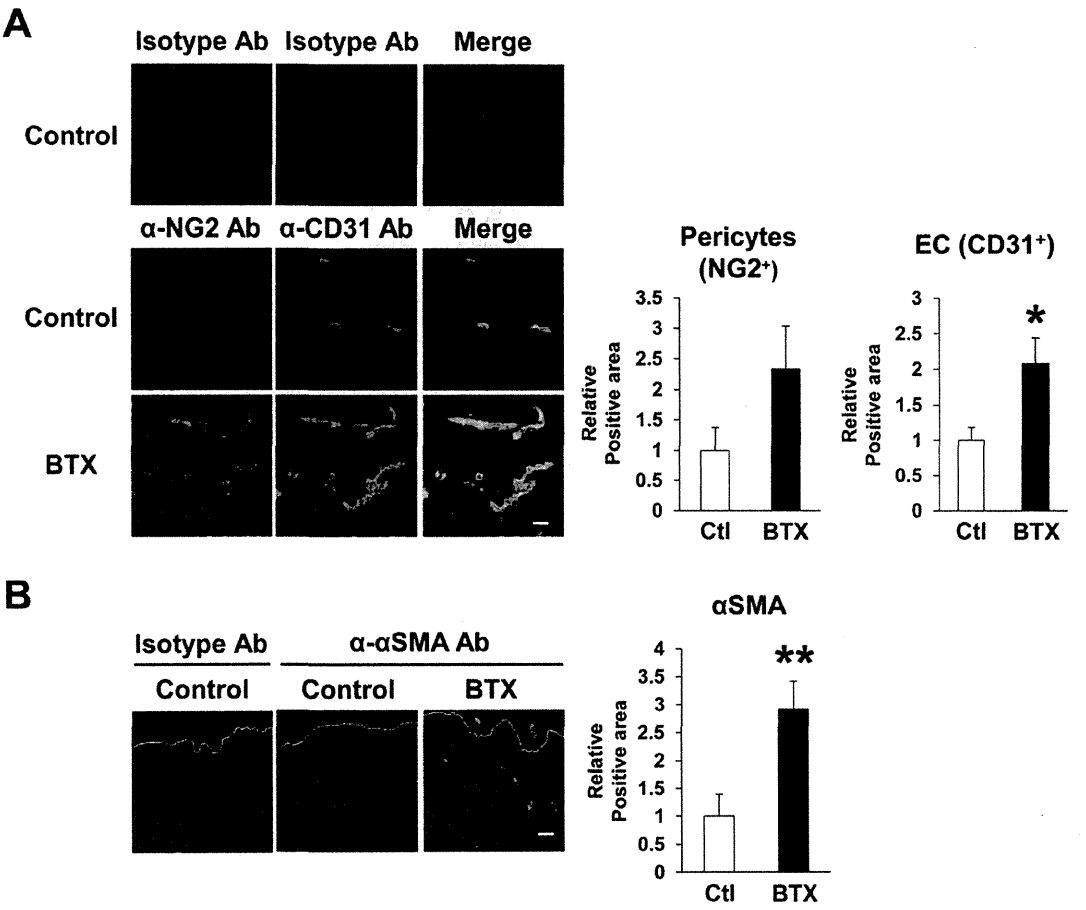

Figure 2 | Botulinum toxin A protected the reduction of vascularity by cutaneous I/R injury. (A) The amount of $CD31^+$ EC and $NG2^+$ pericytes in cutaneous I/R area at 4 days after reperfusion. (B) The amount of αSMA^+ myofibroblast or pericytes in cutaneous I/R area at 4 days after reperfusion. Quantification of the $CD31^+$, $NG2^+$ and αSMA^+ areas in 6 random microscopic fields from the periphery of I/R area in n = 3 mice per groups was performed using Image J software. Positive area in control mice was assigned a value of 1. Values represent mean ± SEM. $^{**}P < 0.01$, $^{*}P < 0.05$. Scale bar = 20 μm.

secondary necrosis, and these responses induce inflammation in the I/R area[31,32]. At first, we examined whether hypoxia and/or oxidative stress are related to the apoptosis in I/R area at 1 day after reperfusion. The stainings of TUNEL and DAPI double-positive nuclei were localized in pimonidazole$^+$ hypoxic area (Figure 5A). In addition, the stainings of TUNEL were co-localized with both DAPI and 8-OHdG (Figure 5B). These results suggest that hypoxia and oxidative stress by I/R injury might be associated with apoptosis in cutaneous I/R area. We next examined the influence of BTX-A on the number of apoptotic cells in the I/R areas in mice. One day after reperfusion, the number of apoptotic cells in the I/R areas in BTX-A-treated mice were significantly lower than those in control mice

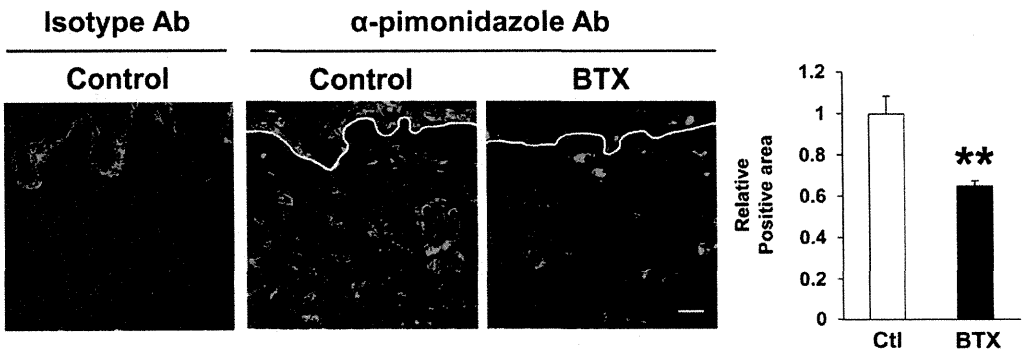

Figure 3 | Botulinum toxin A reduced hypoxic area after cutaneous I/R injury. The amount of pimonidazole$^+$ hypoxic area in cutaneous I/R site at 1 day after reperfusion. Quantification of the pimonidazole$^+$ areas in 8 random microscopic fields from the center of I/R area in n = 3 mice per groups was performed using Image J software. Positive area in control mice was assigned a value of 1. Values represent mean ± SEM. $^{**}P < 0.01$. Scale bar = 20 μm.

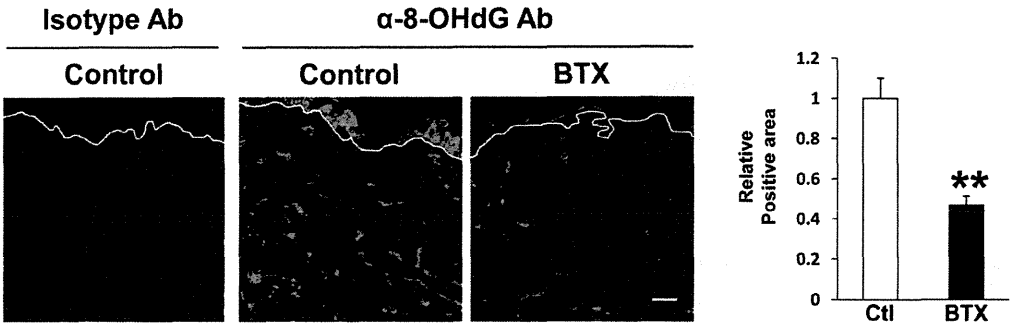

Figure 4 | Botulinum toxin A protected DNA damages after cutaneous I/R injury. The amount of 8-OHdG$^+$ DNA damaged area in cutaneous I/R site at 1 day after reperfusion. Quantification of the 8-OHdG$^+$ areas in 6 random microscopic fields from the center of I/R area in n = 3 mice per groups was performed using Image J software. Positive area in control mice was assigned a value of 1. Values represent mean ± SEM. $^{**}P < 0.01$. Scale bar = 20 μm.

(Figure 5C). These results suggest that BTX-A might reduce the apoptosis induced by cutaneous I/R injury.

Botulinum toxin A reduced the oxidant-induced intracellular accumulation of ROS in vascular endothelial cells. To examine the effects of BTX-A on the oxidative stress affecting vascular endothelial cells, we next examined the effects of BTX-A on H_2O_2-induced intracellular ROS accumulation in vascular endothelial cells using human umbilical vein endothelial cells (HUVECs) *in vitro*. BTX-A suppressed the H_2O_2-induced intracellular ROS accumulation in the HUVECs in a concentration-dependent manner (Figure 6), suggesting that BTX-A might reduce oxidative stress in endothelial cells after I/R injury.

Botulinum toxin A protected against ulcer formation in an intermittent short-time cutaneous I/R injury. We introduced a new cutaneous I/R injury model, which is consisted of three I/R cycles; three-hour period of magnet placement, followed by a reperfusion period of 3 hours, suggesting that this intermittent short-time cutaneous I/R injury may mimic the pathogenesis of RP. Forty percent of the mice developed small skin ulcers after these short I/R cycles by four days after the I/R cycles (Figure 7). The administration of BTX-A completely protected against the ulcer formation after I/R injury (Figure 7). These results confirmed that BTX-A might also prevent the development of cutaneous ulcers induced by the intermittent short-time cutaneous I/R injury.

Discussion

I/R injury induces inflammation, including the infiltration of leukocytes and macrophages and the production of proinflammatory cytokines, and leads to the dysfunction of vascular endothelium, capillary narrowing, vascular infarction and vascular spasm. These vascular damages cause hypoxia and oxidative stress in tissues, resulting in the apoptosis and necrosis of these tissues[1–4]. In the present study, we first assessed the vascular damage induced by I/R injury, and found that the numbers of CD31$^+$ endothelial cells and αSMA$^+$ pericytes or myofibroblasts in I/R areas in BTX-A-treated mice were significantly higher than those in control mice. These results suggest that BTX-A could protect against vascular damages by I/R injury.

The mechanism(s) by which BTX-A protects against the vascular damage induced by I/R injury is unclear. It has been recognized that BTX-A has vasodilatory effects through sympathetic inhibition at the neuromuscular junction. Several previous studies have reported that treatment of the microvasculature with BTX-A causes an increase in the arteriolar diameter and a subsequent increase in blood flow[20–23]. In addition, pre-treatment with BTX-A was associated with a lower rate of arterial and venous thrombosis in an animal model microanastomosis[31]. The damage of the vascular endothelium, including capillary narrowing, vascular infarction and spasm, is associated with the pathogenesis of I/R injury. In addition, endothelium-dependent relaxation is decreased by the damage to the vascular endothelium by I/R injury. These findings suggest that the vasodilation and the inhibition of thrombosis and vasospasm by BTX-A might be involved in the protective effects of BTX-A against the vascular damage caused by I/R injury.

It has been reported that hypoxic insult to vascular endothelial cells by I/R injury resulted in leukocyte-endothelial cell adhesion and neutrophil migration through the endothelial barrier[32,33]. Reactive oxygen species (ROS), such as H_2O_2 and NO, also play essential roles in the tissue damage[4–9]. We herein demonstrated that BTX-A reduced oxidative stress in vascular endothelial cells *in vitro*. These results suggest that BTX-A might protect against the hypoxic insult to the vascular endothelial cells, and these effects mediated by BTX-A might provide us with new insight into the mechanisms by which BTX-A protects against I/R injury. However, further investigations are required to elucidate the precise mechanisms by which BTX-A can reduce oxidative stress.

This is the first investigation to examine the effects of BTX-A against cutaneous I/R injury. Using two experimental conditions and an *in vitro* study, we identified the mechanisms underlying the protective effects of BTX-A against cutaneous I/R injury; (i) protection against the reduction of vascularity by I/R injury, (ii) reduction of the hypoxic area, oxidative stress and apoptosis of cells *in vivo* and (iii) reduction of oxidative stress-induced ROS in vascular endothelial cells *in vitro*. These results suggest that BTX-A might have the potential to prevent the ulcer formation induced by cutaneous I/R injury.

Recently, several studies have reported that the administration of BTX-A significantly improved the symptoms of RP, such as the pain, paresthesia of fingers and digital ulcers[25–30]. One of the mechanisms was reported to be its established acetylcholine-mediated vascular smooth muscle paralysis, which results in the inhibition of spasm and vascular contraction. Another mechanism is thought to be due to the fact that BTX-A inhibits the expression of adrenergic receptors in the vessel walls and blocks the release of norepinephrine and various other neuropeptides, such as calcitonin gene-related peptide (CGRP), glutamate and substance P, which are increased in chronic nerve irritation and pain, and can exacerbate these symptoms[28,29,34,35]. There had previously been no experimental evidence of the beneficial effects of BTX-A against I/R injury associated with RP-induced ulcers using animal models. In this study, we introduced a new experimental condition; an intermittent short-time I/R cutaneous injury. This condition may mimic RP-induced cutaneous ulcers. We demonstrated that the administration of BTX-A completely protected against the ulcer formation after I/R injury. These results confirmed that BTX-A might have preventive and/or therapeutic potential with regard to the development of cutaneous ulcers due to the intermittent I/R as seen in RP.

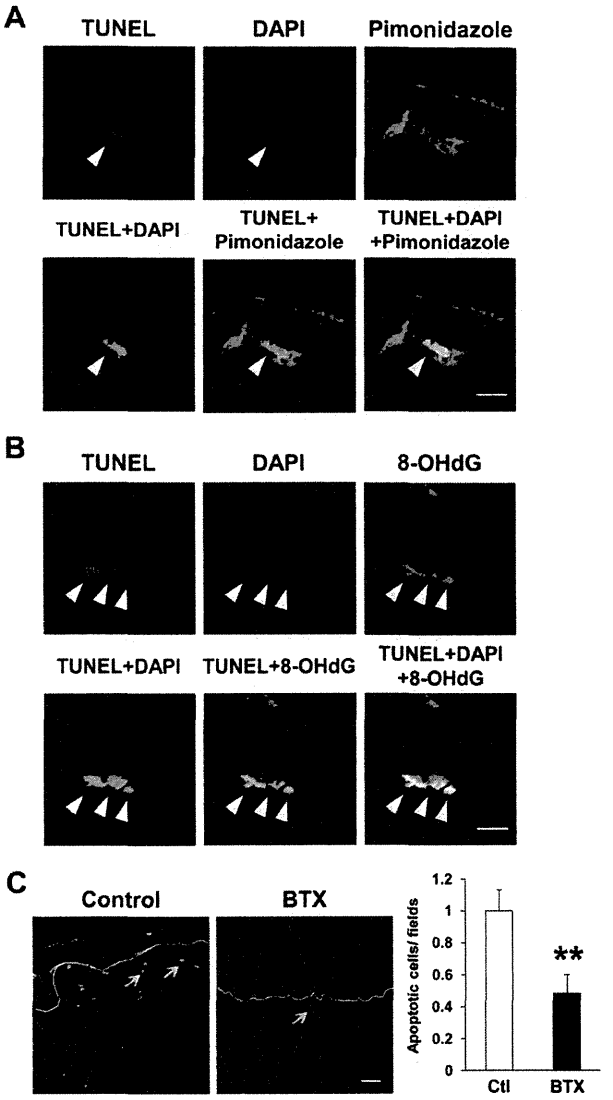

Figure 5 | Botulinum toxin A reduced apoptotic cells after cutaneous I/R injury. (A) Stainings of TUNEL, DAPI and pimonidazole in cutaneous I/R area at 1 day after reperfusion. Stainings of TUNEL and DAPI double-positive nuclei were localized in pimonidazole$^+$ hypoxic area (Arrowhead). Scale bar = 5 μm. (B) Stainings of TUNEL, DAPI and 8-OHdG in cutaneous I/R area at 1 day after reperfusion. Stainings of TUNEL were co-localized with both DAPI and 8-OHdG (Arrowhead). Scale bar = 5 μm. (C) The number of apoptotic cells in I/R site at 1 day after reperfusion was determined by counting both TUNEL and DAPI positive cells (Arrow). Values were determined in 6 random microscopic fields from the center of I/R area in n = 3 mice per groups. The number of apoptotic cells in control mice was assigned a value of 1. Values represent mean ± SEM. $^{**}P < 0.01$. Scale bar = 20 μm.

Taken together, the present findings indicate that BTX-A suppresses the formation of skin ulcers induced by cutaneous I/R injury by protecting against vascular damage, suppressing hypoxia, decreasing oxidative stress and preventing apoptosis. In addition, BTX-A could be expected to be effective for at least three to six months in humans[25–30], therefore, exogenous BTX-A administration has possible long-term preventive and therapeutic potential for patients with cutaneous I/R injuries, including decubitus ulcers and RP-induced digital ulcers.

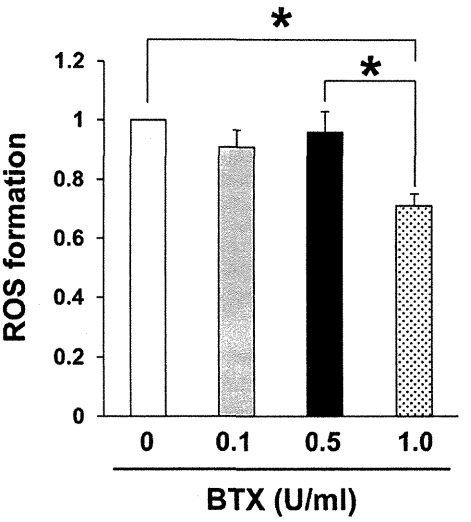

Figure 6 | Botulinum toxin A reduced oxidant-induced intracellular accumulation of ROS in vascular endothelial cells. Quantification of H_2O_2-induced intracellular ROS production in vascular endothelial cells treated with or without BTX. ROS formation in cells without BTX treatment was assigned a value of 1. Values represent mean ± SEM. n = 4 in each group. $^*P < 0.05$.

Methods

Animals. All experiments were approved by the Ethical Committee for Animal Experiments of the Gunma University Graduate School of Medicine, and carried out in accordance with the approved guidelines. C57BL/6 mice were purchased from the SLC (Shizuoka, Japan). Eight- to 12-week-old female mice were used for all experiments. Mice were maintained in the Institute of Experimental Animal Research of Gunma University under specific pathogen-free conditions. Mice were handled in accordance with the animal care guidelines of Gunma University.

Antibodies. Antibodies (Abs) and their sources were as follows: rat anti-mouse CD31 monoclonal Ab (mAb) (MEC13.3; BD Bioscience, San Jose, CA), rabbit anti-mouse NG2 polyclonal Ab (pAb) (Millipore, Billerica, MA), FITC-conjugated mouse anti-αSMA mAb (Sigma, St Louis, MO), goat anti-8-OHdG pAb (abcam, Cambridge, UK). Alexa 488-, Alexa 568-conjugated secondary Abs were obtained from Invitrogen (Carlsbad, CA).

I/R cycles. We used 2 types of cutaneous I/R cycle mice models. The cutaneous I/R model was performed according to previously published protocols[36–38]. Briefly, mice were anesthetized, and hair was shaved and cleaned with 70% ethanol. The dorsal skin was gently pulled up and trapped between two round ferrite magnetic plates that had a 12-mm diameter (113 mm^2) and 5 mm thick, with an average weight of 2.69 g and 1180 G magnetic forces (NeoMag Co, Ichikawa, Japan). Epidermis, dermis, subcutaneous fat layer and subcutaneous loose connective tissue layer, but not

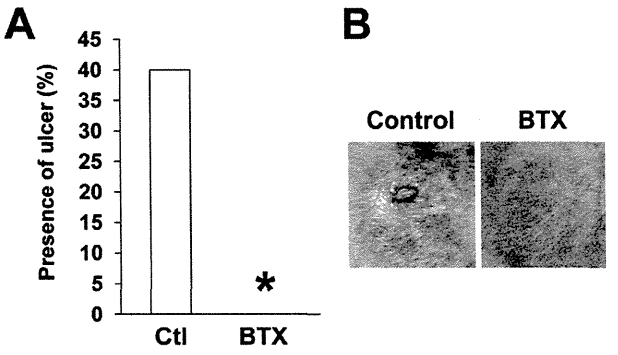

Figure 7 | Botulinum toxin A protected ulcer formation in an intermittent short-time cutaneous I/R injury. (A) The frequency of the presence of skin ulcers in I/R area at 4 days after 3 cycles of I/R injury (n = 10 in each group). $^*P < 0.05$. (B) Photographs of mice back skin after cutaneous I/R in control or BTX treated mice at 4 days after reperfusion.

muscles, were pinched by magnetic plates. This process creates a compressive pressure of 50 mmHg between the two magnets[36,37]. In the analysis of "decubitus ulcer-like cutaneous I/R model", dorsal skin was trapped between magnetic palates for 12 hours, and then plates were removed. Mice were not immobilized, and not anesthetized during ischemia. All of the mice developed two round ulcers separated by a bridge of normal skin. In the analysis of "intermittent short-time cutaneous I/R model", 3 I/R cycles were performed in each mouse. A single IR cycle consisted of a 3-hour period of magnet placement, followed by a release or rest period of 3 hours. To assess the effects of BTX-A (BOTOX VISTA®, Allergan Pharmaceuticals, Irvine, CA) on the development of ulcers after cutaneous I/R injury, 0.5 U or 1.0 U BTX-A per 200 μl 0.9% saline or 200 μl of saline as a control were injected into the dermis in the I/R site 24 hours before the beginning of I/R cycles. For analysis, each wound sites were digitally photographed at the indicated time points after wounding, and wound areas were measured on photographs using Image J (version1.48, NIH, Bethesda, MD) as previously reported[39].

Histological examination and Immunofluorescence staining. Immunofluorescence staining of frozen sections and analyses were performed according to previously described protocols[39,40]. Murine skins were removed and 4 μm frozen sections were prepared and fixed in 4% PFA in PBS for 30 minutes. After blocking with 3% dry milk-PBS supplemented with 5% normal donkey serum or 5% normal goat serum for 1 hour at room temperature, sections were stained with Abs of interest followed by Alexa 488-, Alexa 568-conjugated secondary Abs. Sections were counterstained with 4,6-diamidino-2-phenylindole (DAPI) to visualize nuclei, mounted in ProLong Gold antifade reagent (Invitrogen).

Assessment of tissue hypoxia. Hypoxic areas after cutaneous I/R injury in I/R site were detected using the Hypoxyprobe™-1 Omni kit (Hypoxyprobe, Inc., Burlington, MA) according to the manufacture's protocol. Pimonidazole HCl was injected intraperitoneally (60 mg/kg) 30 minutes before the sacrifice of the mice. Murine skins were removed and 4 μm frozen sections were prepared and fixed cold acetone (4°C) for 10 minutes. Sections were incubated overnight at 4°C with rabbit anti-pimonidazole Ab (PAb2627) diluted 1 : 20 in PBS containing 0.1% bovine serum albumin and 0.1% Tween 20. Sections were incubated for 1 hour with Alexa 488-conjugated secondary Ab. Images (8 fields/section) were taken and visualized with a FV10i-DOC confocal laserscanning microscope (Olympus). The positive area was determined by Image J (version1.48, NIH, Bethesda, MD) in the field (x600) as previously reported[39,40].

ROS detection assay *in vitro*. HUVEC were purchased from ATCC (Manassan, VA). HUVEC were maintained in EBM-2 basal medium (Lonza, Basel, Switzerland) supplemented with EGM-2 Single Quot Kit Suppl. & Growth Factors (Lonza). HUVECs (2.5×10^4 cells) were cultured in OptiPlate™-96F microplate (Perkin Elmer, Waltham, MA). Cells were incubated in the medium with or without BTX-A (0, 0.1, 0.5, 1.0 U/ml FBS(-) DMEM) at 37°C for 24 hours. Cells were stimulated with 0.25 mM H_2O_2 (100 μl/well) for 2 hours, and then ROS levels were measured with DCFDA Cellular ROS Detection Assay Kit (abcam) according to the manufacturer's protocol. Fluorescence was detected by plate reader (Perkin Elmer).

Apoptosis assay. The presence of apoptotic cells in the skin sections were assessed 4 days after reperfusion using terminal deoxynucleotide transferase dUTP nick end-labeling (TUNEL) staining kit (Roche Diagnostics, Indianapolis, IN) according to the manufacturer's protocols. Images (6 fields/section) were taken and visualized with a FV10i-DOC confocal laserscanning microscope (Olympus). The number of apoptotic cells was determined by counting TUNEL and DAPI double positive nuclei in the field (x600) as previously reported[39,40].

Statistical analysis. *P* values were calculated using the Student's *t*-test (two-sided), Chi-square test analysis or by analysis of one-way ANOVA followed by Bonferroni's post test as appropriate. Error bars represent standard errors of the mean, and numbers of experiments (n) are as indicated.

1. Pretto, E. A. Jr. Reperfusion injury of the liver. *Transplant Proc* **23**, 1912–1914 (1991).
2. Woolfson, R. G., Millar, C. G. & Neild, G. H. Ischaemia and reperfusion injury in the kidney: current status and future direction. *Nephrol Dial Transplant* **9**, 1529–314 (1994).
3. Carroll, W. R. & Esclamado, R. M. Ischemia/reperfusion injury in microvascular surgery. *Head Neck* **22**, 700–713 (2000).
4. Kasuya, A., Sakabe, J. & Tokura, Y. Potential application of in vivo imaging of impaired lymphatic duct to evaluate the severity of pressure ulcer in mouse model. *Sci Rep* **4** (2014).
5. Nathan, C. & Xie, Q. W. Nitric oxide synthases: roles, tolls, and controls. *Cell* **78**, 915–918 (1994).
6. Carroll, W. R., Esclamado, R. M. Ischemia/reperfusion injury in microvascular surgery. *Head Neck* **22**, 700–713 (2000).
7. Hayasaki, T. *et al.* CC chemokine receptor-2 deficiency attenuates oxidative stress and infarct size caused by myocardial ischemia-reperfusion in mice. *Circ J* **70**, 342–351 (2006).
8. Furuichi, K., Wada, T. & Iwata, Y. *et al.* CCR2 signaling contributes to ischemia-reperfusion injury in kidney. *J Am Soc Nephrol* **14**, 2503–2515 (2003).
9. Reid, R. R., Sull, A. C., Mogford, J. E., Roy, N. & Mustoe, T. A. A novel murine model of cyclical cutaneous ischemia-reperfusion injury. *J Surg Res* **116**, 172–180 (2004).
10. Salcido, R. *et al.* Histopathology of pressure ulcers as a result of sequential computer-controlled pressure sessions in a fuzzy rat model. *Adv Wound Car* **7**, 23–24 (1994).
11. Peirce, S. M., Skalak, T. C. & Rodeheaver, G. T. Ischemia-reperfusion injury in chronic pressure ulcer formation: a skin model in the rat. *Wound Repair Regen* **8**, 68–76 (2000).
12. Stadler, I., Zhang, R. Y., Oskoui, P., Whittaker, M. S. & Lanzafame, R. J. Development of a simple, noninvasive, clinically relevant model of pressure ulcers in the mouse. *J Invest Surg* **7**, 221–227 (2004).
13. Wigley, F. M. Clinical practice. Raynaud's Phenomenon. *N Engl J Med* **347**, 1001–1008 (2002).
14. Herrick, A. L. The pathogenesis, diagnosis and treatment of Raynaud phenomenon. *Nat Rev Rheumatol* **8**, 469–79 (2012).
15. Maria, G. *et al.* Botulinum toxin injections in the internal anal sphincter for the treatment of chronic anal fissure: long-term results after two different dosage regimens. *Ann Surg* **228**, 664–669 (1998).
16. Schulte-Baukloh, H. Botulinum toxin for neurogenic bladder dysfunction. *Urologe A* **51**, 198–203 (2012).
17. Patel, S. & Martino, D. Cervical dystonia: from pathophysiology to pharmacotherapy. *Behav Neurol* **26**, 275–282 (2013).
18. Winner, P. K., Sadowsky, C. H., Martinez, W. C., Zuniga, J. A. & Poulette, A. Concurrent onabotulinumtoxinA treatment of cervical dystonia and concomitant migraine. *Headache* **52**, 1219–1225 (2012).
19. Olver, J., Esquenazi, A., Fung, V. S., Singer, B. J. & Ward, A. B. Cerebral Palsy Institute. Botulinum toxin assessment, intervention and aftercare for lower limb disorders of movement and muscle tone in adults: international consensus statement. *Eur J Neurol* **17**, 57–73 (2010).
20. Kim, Y. S., Roh, T. S., Lee, W. J., Yoo, W. M. & Tark, K. C. The effect of botulinum toxin A on skin flap survival in rats. *Wound Repair Regen* **17**, 411–417 (2009).
21. Schweizer, D. F. *et al.* Botulinum toxin A and B raise blood flow and increase survival of critically ischemic skin flaps. *J Surg Res* **184**, 1205–1213 (2013).
22. Kim, T. K. *et al.* The effects of botulinum toxin A on the survival of a random cutaneous flap. *J Plast Reconstr Aesthet Surg* **62**, 906–913 (2009).
23. Park, T. H., Rah, D. K., Chong, Y. & Kim, J. K. The Effects of Botulinum Toxin A on Survival of Rat TRAM Flap With Vertical Midline Scar. *Ann Plast Surg* **74**, 100–106 (2015).
24. Küçüker, I. *et al.* The effect of surgical and chemical denervation on ischaemia/reperfusion injury of skeletal muscle. *J Plast Reconstr Aesthet Surg* **65**, 240–248 (2012).
25. Sycha, T., Graninger, M., Auff, E. & Schnider, P. Botulinum toxin in the treatment of Raynaud's phenomenon: a pilot study. *Eur J Clin Invest* **34**, 312–313 (2004).
26. Van Beek, A. L., Lim, P. K., Gear, A. J. & Pritzker, M. R. Management of vasospastic disorders with botulinum toxin A. *Plast Reconstr Surg* **119**, 217–226 (2007).
27. Fregene, A., Ditmars, D. & Siddiqui, A. Botulinum toxin type A: a treatment option for digital ischemia in patients with Raynaud's phenomenon. *J Hand Surg Am* **34**, 446–452 (2009).
28. Neumeister, M. W. *et al.* Botox therapy for ischemic digits. *Plast Reconstr Surg* **124**, 191–201 (2009).
29. Neumeister, M. W. Botulinum toxin type A in the treatment of Raynaud's phenomenon. *J Hand Surg Am* **35**, 2085–2092 (2010).
30. Smith, L., Polsky, D. & Franks, A. G. Jr. Botulinum toxin-A for the treatment of Raynaud syndrome. *Arch Dermatol* **148**, 426–428 (2012).
31. Fathi, M., *et al.* Preventive effect of botulinum toxin A in microanastomotic thrombosis: a rabbit model. *J Plast Reconstr Aesthet Surg* **63**, e720–724 (2010).
32. Eltzschig, H. K. *et al.* Endogenous adenosine produced during hypoxia attenuates neutrophil accumulation: coordination by extracellular nucleotide metabolism. *Blood* **104**, 3986–3992 (2004).
33. Luscinskas, F. W., Ma, S., Nusrat, A., Parkos, C. A. & Shaw, S. K. Leukocyte transendothelial migration: a junctional affair. *Semin Immunol* **14**, 105–113 (2002).
34. Meng, J., Wang, J., Lawrence, G. & Dolly, J. O. Synaptobrevin I mediates exocytosis of CGRP from sensory neurons and inhibition by botulinum toxins reflects their anti-nociceptive potential. *J Cell Sci* **120**, 2864–2874 (2007).
35. Carmichael, N. M., Dostrovsky, J. O. & Charlton, M. P. Peptide-mediated transdermal delivery of botulinum neurotoxin type A reduces neurogenic inflammation in the skin. *Pain* **149**, 316–324 (2010).
36. Peirce, S. M., Skalak, T. C. & Rodeheaver, G. T. Ischemia-reperfusion injury in chronic pressure ulcer formation: a skin model in the rat. *Wound Repair Regen* **8**, 68–76 (2000).
37. Stadler, I., Zhang, R. Y., Oskoui, P., Whittaker, M. S. & Lanzafame, R. J. Development of a simple, noninvasive, clinically relevant model of pressure ulcers in the mouse. *J Invest Surg* **7**, 221–227 (2004).
38. Saito, Y. *et al.* The loss of MCP-1 attenuates cutaneous ischemia-reperfusion injury in a mouse model of pressure ulcer. *J Invest Dermatol* **128**, 1838–1851 (2008).
39. Uchiyama, A. *et al.* MFG-E8 regulates angiogenesis in cutaneous wound healing. *Am J Pathol* **184**, 1981–1990 (2014).

40. Motegi, S. *et al.* Pericyte-derived MFG-E8 regulates pathologic angiogenesis. *Arterioscler Thromb Vasc Biol* **31**, 2024–2034 (2011).

Acknowledgments

This work was supported by Science Research Grant of Clinical Trials Core Hospitals (Gunma University Hospital), institutions selected by Japanese Ministry of Health, Labour and Welfare in fiscal year 2013, Japan (to S.M.).

Author contributions

A.U. and S.M. involved in all the process of planning and implementing the experiment, interpretation of data, and writing the manuscripts. K.Y., B.P., S.O., Y.Y. and Y.T. involved in the process of implementing the experiment. O.I. involved in the process of planning the experiment, interpretation of data, and writing the manuscripts. All authors reviewed the manuscript.

Additional information

Supplementary information accompanies this paper at http://www.nature.com/scientificreports

Competing financial interests: The authors declare no competing financial interests.

How to cite this article: Uchiyama, A. *et al.* Protective effect of botulinum toxin A after cutaneous ischemia-reperfusion injury. *Sci. Rep.* 5, 9072; DOI:10.1038/srep09072 (2015).

JAPANESE DERMATOLOGICAL ASSOCIATION
THE JOURNAL OF DERMATOLOGY

doi: 10.1111/1346-8138.12722

Journal of Dermatology 2014; **41**: 1–4

ORIGINAL ARTICLE

Demographic and clinical features of systemic sclerosis patients with anti-RNA polymerase III antibodies

Sei-ichiro MOTEGI, Sayaka TOKI, Kazuya YAMADA, Akihiko UCHIYAMA, Osamu ISHIKAWA

Department of Dermatology, Gunma University Graduate School of Medicine, Maebashi, Gunma, Japan

ABSTRACT

Anti-RNA polymerase III antibody (RNAP) is primarily detected in diffuse cutaneous type systemic sclerosis (dcSSc) patients and strongly associated with renal crisis. Additionally, there has been increasing evidence that cancer in SSc patients is associated with RNAP. The aim of this study was to examine the demographic and clinical features of SSc patients with RNAP. Among 246 SSc patients, 5.7% were positive for RNAP, 20.7% were positive for anti-topoisomerase I antibody (Topo I) alone and 39.4% were positive for anticentromere antibody (ACA) alone. The modified Rodnan total skin score (mRTSS) in SSc patients with RNAP (19.1 ± 2.6) was significantly higher than those in SSc patients with Topo I (11.5 ± 1.1) and patients with ACA (4.4 ± 0.4). Furthermore, among SSc patients with RNAP, the levels of RNAP were positively correlated with mRTSS. Renal crisis is also significantly more prevalent in SSc patients with RNAP than patients without RNAP. Male sex, dcSSc subtype, digital vasculopathy, including digital ulcers and acro-osteolysis, interstitial lung disease and rheumatoid arthritis complications were prevalent in SSc patients with RNAP and patients with Topo-I. Primary biliary cirrhosis and Sjögren's syndrome were more in SSc patients with RNAP and patients with ACA compared with patients with Topo 1. No significant difference in the frequency of complications, including Raynaud's phenomenon, pulmonary artery hypertension and malignancy was observed between the three groups. Thus, measurement of RNAP in SSc patients is useful for the diagnosis and risk stratification of severe manifestation, such as renal crisis and severe skin sclerosis.

Key words: anti-RNA polymerase III antibody, autoantibody, malignancy, renal crisis, systemic sclerosis.

INTRODUCTION

Systemic sclerosis (SSc) is a connective tissue disorder characterized by fibrosis of the skin and internal organs and microvascular dysfunction.[1] Autoantibodies, such as anti-topoisomerase I antibody (Topo I) and anticentromere antibody (ACA), are useful for the diagnosis of SSc and classification of subtypes. The presence of Topo I is associated with diffuse cutaneous type SSc (dcSSc), while the presence of ACA is associated with limited cutaneous type SSc (lcSSc). It has been recognized that anti-RNA polymerase III antibody (RNAP) is primarily detected in dcSSc patients and strongly associated with renal crisis (RC).[2–6] We recently reported that the demographic and clinical features of SSc patients showed that Topo I positivity and severe skin sclerosis were significantly prevalent in SSc patients with digital ulcers (DU).[7] However, the association of RNAP and digital vasculopathy, such as Raynaud's phenomenon (RP), DU and acro-osteolysis (AO), in SSc patients has not been well characterized. Furthermore, there has been increasing evidence that cancer in SSc patients is associated with RNAP. In this study, we analyzed demographic and clinical features, including digital vasculopathy, organ involvements and the complications of other collagen diseases and cancers, in SSc patients with RNAP.

METHODS

Patients

We analyzed 246 Japanese patients with SSc who visited Gunma University Hospital from 2011 to 2014. All patients fulfilled the criteria for SSc proposed by the American College of Rheumatology.[8] Mean disease duration was 11.8 ± 0.6 years. Patients were classified as having lcSSc or dcSSc according to the classification by LeRoy *et al.*[9] This study was approved by the local research ethics committee of Gunma University. Patients provided written informed consent before participation.

Clinical and laboratory assessments

Skin sclerosis was measured using the modified Rodnan total skin score (mRTSS). Interstitial lung disease (ILD) was detected as bibasilar interstitial fibrosis or a ground-glass shadow visible

Correspondence: Sei-ichiro Motegi, M.D., Ph.D., Department of Dermatology, Gunma University Graduate School of Medicine, 3-39-22 Showa, Maebashi, Gunma 371-8511, Japan. Email: smotegi@gunma-u.ac.jp
Received 11 September 2014; accepted 16 October 2014.

on high-resolution computed tomography scans. Pulmonary artery hypertension (PAH) was defined as an elevated right ventricular systolic pressure (>45 mmHg) by echocardiography, and subsequently, as an elevated mean pulmonary artery pressure (>25 mmHg) by cardiac catheterization. Serum RNAP was measured by enzyme-linked immunosorbent assay kit from MBL (Nagoya, Japan), as previously described.[3,10] The cut-off value was set at 28 according to the manufacturer's recommendation and as previously described.[3,10]

Statistics

Analysis of ANOVA followed by Bonferroni's post-test was used for multiple comparisons. χ^2-Test analysis was used to compare frequencies. Spearman's rank correlation coefficient was used to examine the relationship between two continuous variables. Error bars represent standard errors of the mean.

RESULTS

dcSSc subtype and severe skin sclerosis are associated with SSc patients with RNAP

A total of 246 SSc patients were enrolled in this study, including 78 (31.7%) dcSSc and 168 (68.3%) lcSSc patients. We identified 14 SSc patients with RNAP (5.7%; mean age, 64.1 years; mean disease duration, 9.6 ± 3.1 years) and 232 SSc patients without RNAP (94.3%; mean age, 64.4 years; mean disease duration, 12.0 ± 0.7 years). Among 232 SSc patients without RNAP, 51 SSc patients with Topo I alone (20.7%; mean age, 61.3 years), 97 SSc patients with ACA alone (39.4%; mean age, 66.8 years), six SSc patients double positive for Topo I, ACA or RNP (2.4%; mean age, 68.7 years), 54 SSc patients positive for ANA and negative for Topo I, ACA and RNAP (22%; mean age, 62.5 years), and 24 SSc patients negative for ANA (9.8%; mean age, 63 years) were identified. SSc patients with RNAP, Topo I or ACA are summarized in Table 1. The dcSSc was more frequent in SSc patients with Topo I (78.4%) and SSc patients with RNAP (64.3%) compared with that in SSc patients with ACA (4.1%) (Topo I vs ACA, $P < 0.01$; RNAP vs ACA, $P < 0.01$) (Table 1). Consistent with these results, mRTSS in SSc patients with RNAP (19.1 ± 2.6) and SSc patients with Topo I (11.5 ± 1.1) were significantly higher compared with SSc patients with ACA (4.4 ± 0.4) (RNAP vs ACA, $P < 0.01$; Topo I vs ACA, $P < 0.01$) (Fig. 1a). Interestingly, mRTSS in SSc patients with RNAP was significantly higher compared with SSc patients with Topo I ($P < 0.01$). Furthermore, among SSc patients with RNAP, the levels of RNAP were positively correlated with mRTSS ($P < 0.05$, Fig. 1b). Taken together, these results indicate that the dcSSc subtype and severe skin sclerosis may be significant characteristics of SSc patients with RNAP.

Demographic and clinical features of SSc patients positive for RNAP

The demographic and clinical features of SSc patients positive for RNAP, Topo I and ACA are summarized in Table 1. The proportion of male patients was significantly higher in SSc patients with RNAP and patients with Topo I compared with SSc patients with ACA (RNAP vs ACA, 28.6% vs 4.1%, $P < 0.01$; Topo I vs ACA, 13.7% vs 4.1%, $P < 0.05$).

No significant difference in the frequency of RP was observed between the three groups. The prevalence of DU in SSc patients with RNAP and in patients with Topo I were

Table 1. Demographic and clinical characteristics of SSc patients with anti-RNA polymerase I antibody, anti-topoisomerase I antibody and anticentromere antibody

					P		
	RNAP (n = 14)	Topo I (n = 51)	ACA (n = 97)	Overall *P*-value	RNAP vs Topo I	RNAP vs ACA	Topo I vs ACA
Sex							
Male (%)	28.6 (4/14)	13.7 (7/51)	4.1 (4/97)	<0.01	0.19	<0.01	<0.05
Female (%)	71.4 (10/14)	86.3 (44/51)	95.9 (93/97)				
Type							
lcSSc (%)	35.7 (5/14)	21.6 (11/51)	95.9 (93/97)	<0.01	0.28	<0.01	<0.01
dcSSc (%)	64.3 (9/14)	78.4 (40/51)	4.1 (4/97)				
Complication							
RP (%)	92.9 (13/14)	94.1 (48/51)	94.8 (92/97)	0.95	0.86	0.76	0.85
DU (%)	42.9 (6/14)	37.3 (19/51)	16.5 (16/97)	<0.01	0.7	<0.05	<0.01
PAH (%)	7.1 (1/14)	17.6 (9/51)	8.2 (8/97)	0.2	0.34	0.89	0.09
ILD (%)	78.6 (11/14)	96.1 (49/51)	9.3 (9/97)	<0.01	<0.05	<0.01	<0.01
RC (%)	14.3 (2/14)	0 (0/51)	1 (1/97)	<0.01	<0.01	<0.01	0.47
PBC (%)	14.3 (2/14)	0 (0/51)	15.5 (15/97)	<0.05	<0.01	0.91	<0.01
SjS (%)	28.6 (4/14)	13.7 (7/51)	29.9 (29/97)	0.09	0.19	0.92	<0.05
RA (%)	21.4 (3/14)	15.7 (8/51)	4.1 (4/97)	<0.05	0.61	<0.05	<0.05
Malignancy (%)	7.1 (1/14)	3.9 (2/51)	6.2 (6/97)	0.82	0.61	0.89	0.56

ACA, anticentromere antibody; AO, acro-osteolysis; dcSSc, diffuse cutaneous type of SSc; DU, digital ulcers; ILD, interstitial lung disease; lcSSc, limited cutaneous type of SSc; PAH, pulmonary artery hypertension; PBC, primary biliary cirrhosis; RA, rheumatoid arthritis; RC, renal crisis; RNAP, anti-RNA polymerase III antibody; RP, Raynaud's phenomenon; SjS, Sjögren's syndrome; Topo I, anti-topoisomerase I antibody.

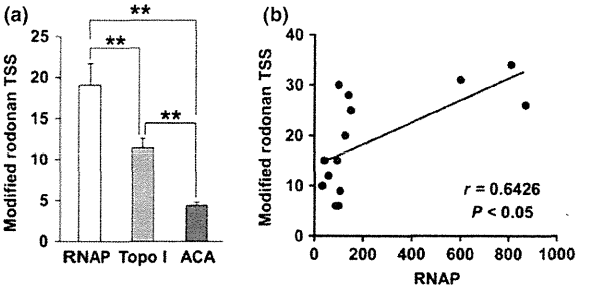

Figure 1. (a) Modified Rodnan total skin score (TSS) in systemic sclerosis (SSc) patients with anti-RNA polymerase III antibody (RNAP: $n = 14$, 20.4 ± 3.1), anti-topoisomerase I antibody (Topo I: $n = 51$, 11 ± 1.1) and anticentromere antibody (ACA: $n = 97$, 4.4 ± 0.4). Values represent mean ± standard error of the mean (**$P < 0.01$). (b) Correlation of anti-RNA polymerase III antibody (RNAP) levels with modified Rodnan total skin score (TSS) in SSc patients with RNAP. Solid line represents the regression line. RNAP levels significantly correlated with modified Rodnan TSS ($r = 0.6426$, $P < 0.05$, Spearman's rank correlation coefficient).

significantly higher compared with SSc patients with ACA (RNAP vs ACA, 42.9% vs 16.5%, $P < 0.05$; Topo I vs ACA, 37.3% vs 16.5%, $P < 0.01$). AO, the resorption of the terminal tuft of the digit, is a characteristic feature in SSc, and AO is caused by severe digital ischemia, including RP and chronic vasculopathy.[11] The prevalence of AO in SSc patients with RNAP tends to be higher than in patients with ACA, but this difference was not statistically significant (RNAP vs ACA, 14.3% vs 4.1%, $P = 0.12$). The prevalence of AO in SSc patients with Topo I was significantly higher compared with SSc patients with ACA (Topo I vs ACA, 13.7% vs 4.1%, $P < 0.05$). These results suggest that the prevalence of digital vasculopathy in SSc patients with RNAP may be similar to those in patients with Topo I rather than those in patients with ACA.

No significant difference in the frequency of PAH was observed between the three groups. The prevalence of ILD in SSc patients with RNAP and in SSc patients with Topo I was also significantly higher than that in SSc patients with ACA (RNAP vs ACA, 78.6% vs 9.3%, $P < 0.01$; Topo I vs ACA, 96.1% vs 9.3%, $P < 0.01$). The prevalence of RC in SSc patients with RNAP was also significantly higher than that in SSc patients without RNAP (RNAP vs Topo I, 14.3% vs 0%, $P < 0.01$; RNAP vs ACA, 14.3% vs 1%, $P < 0.01$). The complication of primary biliary cirrhosis (PBC) and Sjögren's syndrome (SjS) was more frequent in SSc patients with RNAP and SSc patients with ACA than in SSc patients with Topo I (PBC: RNAP vs Topo I, 14.3% vs 0%, $P < 0.01$; ACA vs Topo I, 15.5% vs 0%, $P < 0.01$) (SjS: RNAP vs Topo I, 28.6% vs 13.7%, $P = 0.19$; ACA vs Topo I, 29.9% vs 13.7%, $P < 0.05$). Rheumatoid arthritis (RA) was more frequent in SSc patients with RNAP and SSC patients with Topo I than in SSc patients with ACA (RNAP vs ACA, 21.4% vs 4.1%, $P < 0.05$; Topo I vs ACA, 15.7% vs 4.1%, $P < 0.05$). No significant difference in the frequency of malignancy was observed between the three groups. These results suggest that the presence of RNAP may help to predict organ involvements and the complications of other collagen diseases in SSc patients.

Because severe skin sclerosis was treated with corticosteroids, the rate of the treatment with corticosteroids in SSc patients with RNAP was significantly higher compared with that in patients without RNAP (71.4% [10/14] vs 24.1% [56/232], $P < 0.01$). In addition, the rate of the treatment with i.v. prostanoid, such as lipoprostaglandin E1, in SSc patients with RNAP was significantly higher compared with that in patients without RNAP (28.6% [4/14] vs 7.3% [17/232], $P < 0.01$). In contrast, no significant differences in the rate of antiplatelet agents (42.9% [6/14] vs 35.8% [83/232], $P = 0.59$), oral prostanoid (71.4% [10/14] vs 63.8% [148/232], $P = 0.56$) and endothelin receptor antagonist bosentan (14.3% [2/14] vs 5.6% [13/232], $P = 0.19$) were observed between the two groups.

DISCUSSION

The positive rate of RNAP in SSc patients varies in previous studies; 26.6% of 2177 patients in the UK,[12] 19.4% of 242 patients in Canada,[4] 15.3% of 451 patients in Australia,[6] 15.3% of 196 patients in the USA,[2] 9.4% of 319 patients in France[5] and 4.4% of 360 patients in Italy.[13] In the studies of Japanese SSc patients, 10.7% of 354 patients,[3] 6.4% of 265 patients[2] and 5.9% of 203 patients[14] were positive for RNAP. In our study, 5.7% of 246 SSc patients was positive for RNAP, suggesting that the prevalence of RNAP in Japanese patients appears to be lower than in North American and English patients, and that ethnicity or lifestyle may account for the variety of positivity rates for RNAP.

Previous studies have reported the associations of RNAP with diffuse cutaneous type, higher maximum skin thickness score, tendon friction rubs and renal crisis.[2–6] Our SSc patients with RNAP were also associated with high mRTSS and renal crisis, being consistent with previous results. The awareness of high risk for renal crisis by the detection of RNAP is essential to establish an early correct diagnosis of renal crisis and to perform early appropriate treatment.

We found that the levels of RNAP were positively correlated with mRTSS in SSc patients with RNAP. Kuwana *et al.*[2] reported that RNAP levels were serially analyzed for more than 8 years in six RNAP-positive SSc patients and that RNAP levels were closely correlated with the total skin score in four patients with RNAP. In addition, Tanahashi *et al.*[15] reported that RNAP levels become negative after successful treatment in SSc patients with RNAP. These findings suggested that RNAP may be useful in evaluating disease activity, and that serial measurement of RNAP in SSc patients may be useful for predicting disease progression and the onset of renal crisis.

There are few studies on the association of RNAP and digital angiopathy, and no association of RNAP with DU has been reported.[3,6] In our study, the prevalence of DU in SSc patients with RNAP and in patients with Topo I were significantly higher compared with SSc patients with ACA. We previously reported

that all RNAP-positive SSc patients with DU had DU at the extensor surface of the joints, suggesting that RNAP positivity was more frequent in SSc patients with DU at the extensor surface of joints.[7] Because DU at the extensor surface of the joints may be predominantly caused by a contracture of the phalanges due to severe skin sclerosis and minor trauma, severe skin sclerosis rather than digital angiopathy may be responsible for DU in SSc patients with RNAP.

Several studies have pointed out that there is an association with cancer in SSc patients with RNAP and the onset of SSc. A cohort study of 360 Italian patients with SSc demonstrated that malignancies were more frequent in the RNAP group (7/16 patients) compared with the Topo I (11/101) and ACA groups (21/243) ($P < 0.001$).[13] Among the SSc patients who were diagnosed with cancer within 6 months before to 12 months after the onset of SSc, there were more patients with RNAP (3/16 patients) than patients with Topo I (0/101) or ACA (1/243).[13] These findings suggested a significant association between malignancies synchronous with SSc onset and positive for RNAP. Other large studies of SSc patients in France, Australia and the UK have also reported similar results.[5,6,12] Shah *et al.*[16] demonstrated that exclusive nucleolar staining of RNA polymerase III was detected in four out of five ovary or breast cancers from SSc patients with RNAP and suggested that tumor antigen expression and SSc autoantibodies were closely associated, and that malignancy may initiate the scleroderma-specific immune response and drive disease in a subset of SSc patients. In our study, only one patient with RNAP had lung cancer, which occurred 29 years after the diagnosis of SSc. Our SSc patients with RNAP were not significantly associated with malignancy. Because the SSc patients were collected until recently (2014) in this study, there is the limitation that the follow-up period may not be long enough for analysis of demographic and clinical features, especially malignancy, in SSc patients with RNAP. Therefore, a longer follow-up period and more patients are required to assess the association of malignancy with RNAP, and careful survey of malignancy in SSc patients with RNAP is required.

In conclusion, we found that severe skin sclerosis and renal crisis was significantly more prevalent in SSc patients with RNAP and that the level of RNAP was positively correlated with the total skin score, suggesting that the measurement of RNAP in SSc patients may be useful for the diagnosis and risk stratification of a severe manifestation.

CONFLICT OF INTEREST: The authors declare that there are no conflicts of interest.

REFERENCES

1 Asano Y. Future treatments in systemic sclerosis. *J Dermatol* 2010; **37**: 54–70.
2 Kuwana M, Okano Y, Pandey JP *et al.* Enzyme-linked immunosorbent assay for detection of anti-RNA polymerase III antibody: analytical accuracy and clinical associations in systemic sclerosis. *Arthritis Rheum* 2005; **52**: 2425–2432.
3 Satoh T, Ishikawa O, Ihn H *et al.* Clinical usefulness of anti-RNA polymerase III antibody measurement by enzyme-linked immunosorbent assay. *Rheumatology (Oxford)* 2009; **48**: 1570–1574.
4 Santiago M, Baron M, Hudson M, Burlingame RW, Fritzler MJ. Antibodies to RNA polymerase III in systemic sclerosis detected by ELISA. *J Rheumatol* 2007; **34**: 1528–1534.
5 Meyer O, De Chaisemartin L, Nicaise-Roland P *et al.* Anti-RNA polymerase III antibody prevalence and associated clinical manifestations in a large series of French patients with systemic sclerosis: a cross-sectional study. *J Rheumatol* 2010; **37**: 125–130.
6 Nikpour M, Hissaria P, Byron J *et al.* Prevalence, correlates and clinical usefulness of antibodies to RNA polymerase III in systemic sclerosis: a cross-sectional analysis of data from an Australian cohort. *Arthritis Res Ther* 2011; **13**: R211.
7 Motegi S, Toki S, Hattori T *et al.* No association of atherosclerosis with digital ulcers in Japanese patients with systemic sclerosis: evaluation of carotid intima-media thickness and plaque characteristics. *J Dermatol* 2014; **41**: 604–608.
8 Subcommittee for Scleroderma Criteria of the American Rheumatism Association Diagnostic and Therapeutic Criteria Committee. Preliminary criteria for the classification of systemic sclerosis (scleroderma). *Arthritis Rheum* 1980; **23**: 581–590.
9 LeRoy EC, Black C, Fleischmajer R *et al.* Scleroderma (systemic sclerosis): classification, subsets and pathogenesis. *J Rheumatol* 1988; **15**: 202–205.
10 Kuwana M, Kimura K, Kawakami Y. Identification of an immunodominant epitope on RNA polymerase III recognized by systemic sclerosis sera: application to enzyme-linked immunosorbent assay. *Arthritis Rheum* 2002; **46**: 2742–2747.
11 Johnstone EM, Hutchinson CE, Vail A, Chevance A, Herrick AL. Acro-osteolysis in systemic sclerosis is associated with digital ischaemia and severe calcinosis. *Rheumatology (Oxford)* 2012; **51**: 2234–2238.
12 Moinzadeh P, Fonseca C, Hellmich M *et al.* Association of anti-RNA polymerase III autoantibodies and cancer in scleroderma. *Arthritis Res Ther* 2014; **16**: R53.
13 Airo' P, Ceribelli A, Cavazzana I *et al.* Malignancies in Italian patients with systemic sclerosis positive for anti-RNA polymerase III antibodies. *J Rheumatol* 2011; **38**: 1329–1334.
14 Hamaguchi Y, Hasegawa M, Fujimoto M *et al.* The clinical relevance of serum antinuclear antibodies in Japanese patients with systemic sclerosis. *Br J Dermatol* 2008; **158**: 487–495.
15 Tanahashi K, Sugiura K, Muro Y, Akiyama M. Disappearance of circulating autoantibodies to RNA polymerase III in a patient with systemic sclerosis successfully treated with corticosteroid and methotrexate. *J Eur Acad Dermatol Venereol* 2014. doi: 10.1111/jdv.12512.
16 Shah AA, Rosen A, Hummers L, Wigley F, Casciola-Rosen L. Close temporal relationship between onset of cancer and scleroderma in patients with RNA polymerase I/III antibodies. *Arthritis Rheum* 2010; **62**: 2787–2795.

Protective Effect of MFG-E8 after Cutaneous Ischemia–Reperfusion Injury

Akihiko Uchiyama[1], Kazuya Yamada[1], Buddhini Perera[1], Sachiko Ogino[1], Yoko Yokoyama[1], Yuko Takeuchi[1], Osamu Ishikawa[1] and Sei-ichiro Motegi[1]

We recently demonstrated that the secreted glycoprotein and integrin-ligand MFG-E8 promotes cutaneous wound healing by enhancing angiogenesis. Several studies have identified potential roles for MFG-E8 in regulation of ischemia–reperfusion (I/R) injury in the brain, kidney, and liver. Our objective was to assess the role of MFG-E8 in the formation of skin ulcers using a murine model of cutaneous I/R injury–cutaneous pressure ulcers. Cutaneous I/R was performed by trapping the dorsal skin between two magnetic plates for 12 hours, followed by plate removal. Expression of MFG-E8 increased in the dermis during ischemia, and then decreased after reperfusion. Administration of recombinant (r)MFG-E8 in I/R areas at the beginning of reperfusion significantly inhibited the formation of cutaneous pressure ulcers, and the number of $CD31^+$ vessel and $NG2^+$ pericytes in wounds were increased in I/R mice treated with rMFG-E8. The number of M1 macrophages and the amount of proinflammatory mediators monocyte chemotactic protein-1,induced nitric oxide synthase, IL-6, tumor necrosis factor-α, and IL-1β in the wound area were reduced by the administration of rMFG-E8. We conclude that MFG-E8 may inhibit the formation of pressure ulcers induced by cutaneous I/R injury by regulating angiogenesis and inflammation. Exogenous application of MFG-E8 might have therapeutic potential for cutaneous I/R injuries, including decubitus ulcers and Raynaud's phenomenon–induced digital ulcers.

Journal of Investigative Dermatology advance online publication, 8 January 2015; doi:10.1038/jid.2014.515

INTRODUCTION

Pressure ulcers are increasing over the world owing to aging of the population. Pressure ulcers are significant sources of pain and distress, leading to the impairment of the quality of life of patients (Gorecki *et al.*, 2009). Although it has long been considered that chronic tissue ischemia was a primary factor in the pathogenesis of pressure ulcers, there has been increasing evidence that ischemia–reperfusion (I/R) is associated with the pathogenesis of pressure ulcers (Salcido *et al.*, 1994; Peirce *et al.*, 2000; Stadler *et al.*, 2004). Many studies of I/R injury in various organs, including the brain, kidney, and liver, suggested that the pathogenesis of I/R injury was quite complex and different from that of the injury by chronic ischemia (Carden and Granger, 2000). I/R injury is defined as a cellular injury caused by the reperfusion of blood to previously ischemic tissue, and the cascade of harmful events, including dysfunction of endothelial cells, edema, capillary narrowing, leukocyte and macrophage infiltration, production of proinflammatory cytokines, and, thereafter, the apoptosis and necrosis of tissues (Pretto 1991; Wolfson et al., 1994). Therefore, I/R injury causes more severe tissue damage compared with ischemia alone (Carden and Granger, 2000; Carmo-Araújo et al., 2007). Reactive oxygen species also have essential roles in tissue damage by reperfusion. Nitric oxide (NO) is one of the reactive oxygen species, and excessive NO or its synthase, inducible NO synthase (iNOS), is associated with the pathogenesis of I/R-induced apoptosis and tissue injury (Nathan and Xie, 1994; Reid *et al.*, 2004; Kasuya *et al.* 2014). Saito *et al.*,(2008) reported that cutaneous I/R induced the recruitment of neutrophils and macrophages and the subsequent release of proinflammatory cytokines, including IL-1β, IL-6, and tumor necrosis factor-α (TNF-α), and toxic oxygen-derived free radicals induced the apoptosis of skin fibroblasts and skin injury. In addition, they reported that monocyte chemoattractant protein-1 (MCP-1) was an important factor for macrophage recruitment and it had a role in apoptosis and injury via inducing iNOS during reperfusion rather than the ischemic period (Saito *et al.*, 2008).

The secreted glycoprotein MFG-E8, also called lactadherin and SED1, is composed of two N-terminal EGF-like domains and two C-terminal discoidin-like domains (C1 and C2) that share homology with blood coagulation factors V and VIII (Stubbs *et al.*, 1990; Ogura *et al.*, 1993). One EGF-like domain (E2) contains RGD integrin-binding motif, and MFG-E8 binds

[1]*Department of Dermatology, Gunma University Graduate School of Medicine, Maebashi, Japan*

Correspondence: Sei-ichiro Motegi, Department of Dermatology, Gunma University Graduate School of Medicine, 3-39-22, Showamachi, Maebashishi, Gunma 371-8511, Japan. E-mail: smotegi@gunma-u.ac.jp

Abbreviations: I/R, ischemia–reperfusion; iNOS, induced nitric oxide synthase; KO, knockout; NO, nitric oxide; PDGF, platelet-derived growth factor; PDGFRβ, PDGF receptor β; rMFG-E8, recombinant MFG-E8; RT–PCR, reverse transcriptase–PCR; siRNA, small interfering RNA; TNF-α, tumor necrosis factor-α; WT, wild type

Received 12 August 2014; revised 29 November 2014; accepted 1 December 2014; accepted article preview online 10 December 2014

to integrin αvβ3/5 (Andersen *et al.*, 1997; Taylor *et al.*, 1997; Hanayama *et al.*, 2002). MFG-E8 acts as a bridging protein between phosphatidylserine on the surface of apoptotic cells and integrin αvβ3/5 on the surface of phagocytes, and it enhances the phagocytosis and clearance of apoptotic cells (Hanayama *et al.*, 2002; Asano *et al.*, 2004).

With respect to the regulation of angiogensis, there are several reports stating that the interactions of MFG-E8 with integrin αv have been implicated in the enhancement of angiogenesis in mice (Silvestre *et al.*, 2005; Neutzner *et al.*, 2007). Recently, we demonstrated that pericytes and/or pericyte precursors were important sources of MFG-E8 in melanoma tumors in mice, and that MFG-E8 enhanced angiogenesis in melanoma tumors and in oxygen-induced retinopathy in mice (Motegi *et al.*, 2011a). We have also determined that MFG-E8 associated with integrin αv and platelet-derived growth factor receptor β (PDGFRβ) on the surface of pericytes after platelet-derived growth factor (PDGF) treatment, and inhibited PDGF-stimulated degradation of PDGFRβ, resulting in the enhancement of PDGFRβ signaling mediated by integrin–growth factor receptor cross talk (Motegi *et al.*, 2011b). Moreover, we recently demonstrated that MFG-E8 is important for cutaneous wound healing using a mouse model with full-thickness cutaneous wounds (Uchiyama *et al.*, 2014), in which MFG-E8 was increased in granulation tissue in cutaneous wound area. Wound healing was significantly delayed in MFG-E8 knockout (KO) mice compared with wild-type (WT) mice, and recombinant mouse MFG-E8 (rMFG-E8) treatment enhanced wound healing in MFG-E8 KO mice. These results suggest that MFG-E8 could be effectively targeted with therapeutic benefit for the wound caused by ischemic disorders.

Recent studies revealed that MFG-E8 significantly reduces inflammation and protects tissue injury after I/R in several organs including the brain, liver, kidney, and gut (Matsuda *et al.*, 2011; Wu *et al.*, 2012; Deroide *et al.*, 2013; Matsuda *et al.*, 2013). These studies demonstrated that MFG-E8 mRNA and protein expression in organs, including kidney, liver, and gut, were significantly decreased by I/R, and that treatment with rMFG-E8 recovered organ dysfunction and suppressed inflammatory responses. From these previous findings and our results, we hypothesized that treatment with rMFG-E8 might prevent tissue damage and promote angiogenesis in cutaneous I/R injury. However, the possible role of MFG-E8 in cutaneous I/R injury has not been studied previously. Herein, we analyzed changes of the expression of MFG-E8 in cutaneous I/R injury, and the effect of the treatment with rMFG-E8 in cutaneous I/R injury of mouse skin.

RESULTS

Expression of MFG-E8 during cutaneous I/R *in vivo*

To investigate the effect of cutaneous I/R injury on MFG-E8 expression *in vivo*, mRNA levels of MFG-E8 expression in the skin of I/R sites during I/R injury were analyzed. Levels of MFG-E8 mRNA increased in the skin during ischemia by 2.5-fold compared with that before I/R, and then immediately decreased to the basal levels at 4 hours after reperfusion, followed by a gradual decrease by 0.5-fold at 72 hours after reperfusion compared with that before I/R (Figure 1a). These results suggest that MFG-E8 expression was enhanced by hypoxic condition owing to the ischemia.

To assess which kinds of cells in skin can contribute to the increased MFG-E8 expression during ischemia, we performed immunofluorescence staining of MFG-E8 in skin before ischemia (−12 hours), just after reperfusion (0 hour), and 72 hours after reperfusion (72 hours). We determined that MFG-E8 expression around $CD31^+$ ECs and αSMA^+ (α-smooth muscle actin) pericytes/vascular smooth muscle cells (SMCs) just after reperfusion (0 hour) was enhanced compared with that before ischemia (−12 hours) and 72 hours after reperfusion (72 hours; Figure 1b). These results suggest that ECs and pericytes/vascular SMCs might be primary sources of MFG-E8 during ischemia.

Expression of MFG-E8 in pericyte-like cells, endothelial cells, and fibroblasts treated with hypoxic condition *in vitro*

We previously determined that pericytes were the major sources of MFG-E8 in B16 melanoma tumors, and that MFG-E8 localized in close proximity to pericytes/vascular SMCs in the dermis of murine and human skin (Motegi *et al.*, 2011a; Uchiyama *et al.*, 2014). In addition, immunofluorescence staining of skin in the I/R site showed that the MFG-E8 expression levels around blood vessels were enhanced during ischemia. Therefore, we next examined whether hypoxic condition enhanced the expression of MFG-E8 in pericytes, ECs, and fibroblasts *in vitro*. In 10T1/2 cells, which are surrogates for pericytes and pericyte precursors, MFG-E8 mRNA levels were significantly enhanced by hypoxia in a time-dependent manner (Figure 1c). MFG-E8 mRNA levels in ECs (human umbilical vein endothelial cells) were also significantly enhanced by hypoxia in a time-dependent manner (Figure 1c). MFG-E8 mRNA levels in fibroblasts (NIH3T3) were significantly enhanced by hypoxia for 1 hour, but were not changed by hypoxia for 12 hours. In addition, in immunoblots of whole-cell lysates, protein levels of MFG-E8 expression in 10T1/2 cells were also increased by hypoxic conditions (Figure 1d). These results suggest that ischemia-induced hypoxia in the skin may enhance the expression of MFG-E8 in pericytes/vascular SMCs and ECs in I/R sites.

rMFG-E8 protected ulcer formation after cutaneous I/R

To assess the effect of rMFG-E8 on cutaneous pressure ulcers after I/R *in vivo*, we compared the wound area after I/R injury in normal C57BL/6 mice treated with subcutaneous injection of rMFG-E8 or phosphate-buffered saline as a control. We used a simple, reproducible, and noninvasive experimental mouse model to evaluate the pathogenesis of cutaneous pressure ulcers by I/R *in vivo* (Stadler *et al.*, 2004; Saito *et al.*, 2008). Administration of rMFG-E8 significantly inhibited the formation of cutaneous pressure ulcers after I/R (Figure 2a and b). At 3 days after reperfusion, wound areas in rMFG-E8-treated mice were 60% of the wound areas in control mice. Wound areas in rMFG-E8-treated mice were significantly smaller than those in control mice from 1 to 8 days after reperfusion. The wound closure time in control mice was

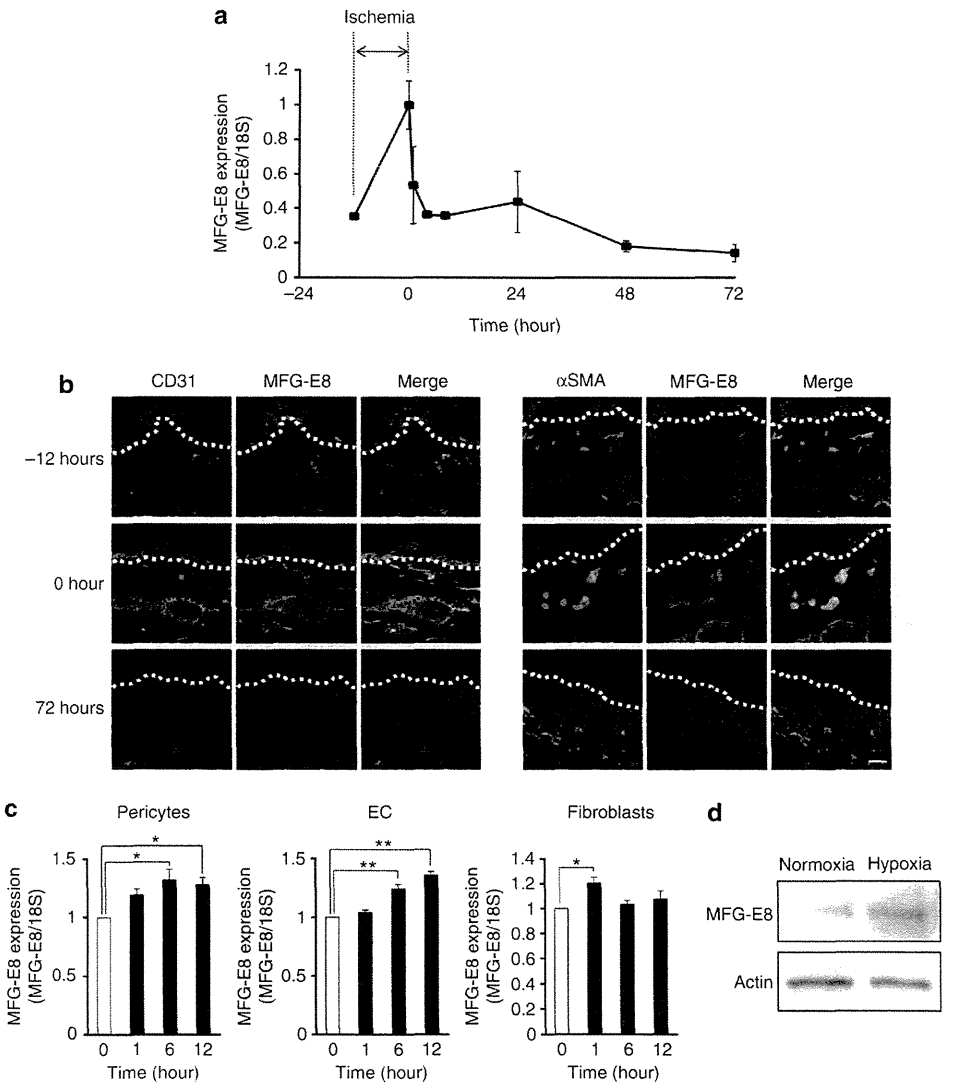

Figure 1. MFG-E8 mRNA expression during ischemia–reperfusion (I/R) injury and hypoxia treatment. (**a**) Quantification of MFG-E8 mRNA levels in the I/R site from the beginning of ishemia to 72 hours after reperfusion by quantitative reverse transcriptase–PCR (RT–PCR). The end of ischemia was assigned 0. Data are relative to mRNA level in 0 h. Values were determined in n = 3 mice. (**b**) Expression and distribution of MFG-E8 in the skin during I/R injury (−12 hours: before ischemia, 0 hour: just after reperfusion, 72 hours: 72 hours after reperfusion). Scale bar = 20 μm. Data are representative of $n = 3$ independent experiments. (**c**) Quantification of MFG-E8 mRNA levels in pericytes, endothelial cells, and fibroblasts by quantitative RT–PCR. Cells were treated with hypoxia for the indicated times. The amount of MFG-E8 expression in nontreated cells was assigned a value of 1. Values were determined in three independent experiments. $^{**}P < 0.01$, $^{*}P < 0.05$ relative to nontreated cells. (**d**) MFG-E8 protein levels in 10T1/2 cells by immunoblotting. 10T1/2 cells were treated with hypoxia or normoxia conditions for 24 hours. Data are representative of $n = 3$ independent experiments.

significantly longer than that in rMFG-E8-treated mice. These results demonstrate that rMFG-E8 partially protected the formation of cutaneous pressure ulcers after I/R.

To further examine the protective effect of MFG-E8 on I/R injury, we compared the wound area after I/R in MFG-E8 WT and KO mice. Wound areas in the MFG-E8 KO mice tended to be larger than those in WT mice. At 2 days after reperfusion, wound areas in MFG-E8 KO mice were significantly larger than those in WT mice (Figure 2c). This result may partially support the results that rMFG-E8 injection protected against cutaneous I/R injury.

rMFG-E8 suppressed infiltrating macrophages, especially M1 macrophages, into cutaneous I/R area

Infiltrating neutrophils and macrophages participate in I/R injury by regulating inflammation and angiogenesis. Therefore, we next analyzed the effect of rMFG-E8 on infiltrating neutrophils and macrophages after cutaneous I/R injury. At 1 day after reperfusion, the prominent edema in the dermis and the infiltration of inflammatory cells in the hypodermis were histologically observed (data not shown). The numbers of infiltrating MPO^+ neutrophils in control mice were comparable to those in rMFG-E8-treated mice at 1 day after

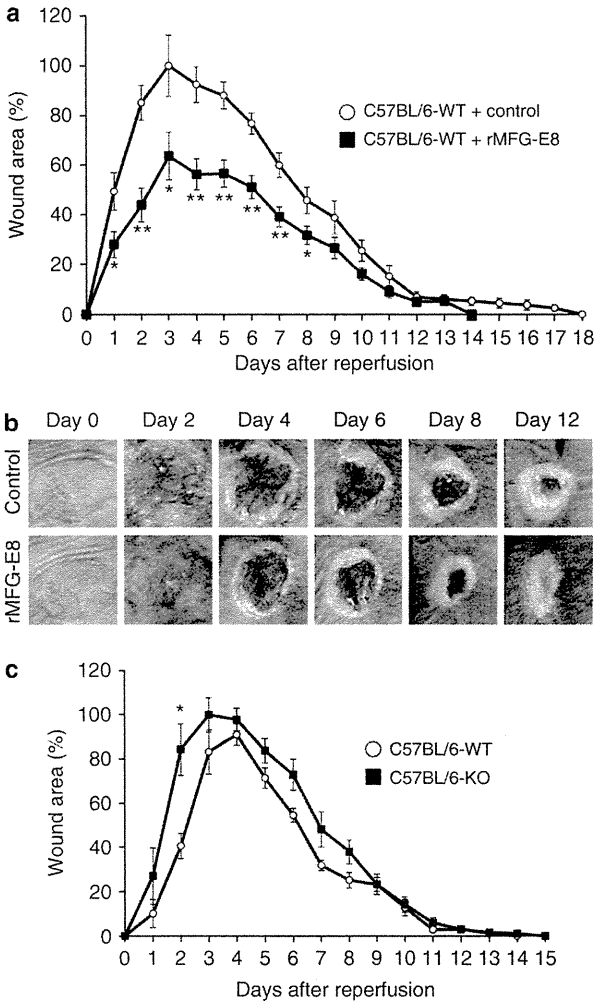

Figure 2. rMFG-E8 protected pressure ulcer formation after cutaneous ischemia–reperfusion (I/R). (**a**) The size of the wound area after I/R injury in normal C57BL/6 mice treated with subcutaneous injection of rMFG-E8 or phosphate-buffered saline as a control. The size of the ulcer in control mice at 3 days after reperfusion was assigned a value of 100% (Control: $n = 10$, rMFG-E8: $n = 10$, for each time point and group). $^{**}P < 0.01$, $^{*}P < 0.05$. (**b**) Photographs of the wound after cutaneous I/R in control or rMFG-E8 mice at 0, 2, 4, 6, 8, and 12 days after reperfusion. (**c**) The size of the wound area after I/R injury in MFG-E8 wild-type (WT) and KO (knockout) mice. The size of the ulcer in WT mice at 3 days after reperfusion was assigned a value of 100%. $n = 5$ mice per genotype. $^{*}P < 0.05$.

reperfusion (Figure 3a). However, the numbers of $CD68^+$ macrophages in rMFG-E8-treated mice were significantly decreased (Figure 3b), suggesting that rMFG-E8 might regulate accumulation or functions of macrophages.

Local microenvironment influences the phagocytic and secretory behavior of macrophages to promote the development of either classically activated macrophages (M1 macrophages) or alternatively activated macrophages (M2 macrophages; Lawrence and Natoli, 2011; Ferrante and Leibovich, 2011). M1 macrophages are observed in initial tissue damage responses, and they induce inflammation by the secretion of proinflammatory mediators, including MCP-1, NO, IL-1, IL-6, IL-12, and TNF-α (Mosser, 2003; Lawrence and Natoli, 2011). M2 macrophages have an essential role in early and middle stages of wound healing, and they induce the resolution of inflammation and promote tissue repair. Therefore, we next examined the numbers of M1/M2 macrophages in I/R areas. The number of total $CD68^+$ macrophages and $CD68^+$, $iNOS^+$ M1 macrophages in I/R areas in rMFG-E8-treated mice were significantly reduced compared with those in control mice (Figure 3c). In addition, the numbers of $CD68^+$, arginase-1^+ M2 macrophages in the I/R area in rMFG-E8-treated mice were significantly reduced (Figure 3d). mRNA levels of iNOS and arginase-1 in I/R areas in rMFG-E8-treated mice were also significantly reduced (Figure 3e). Although M1 macrophage/total macrophage ratios in the wound area in rMFG-E8-treated mice were reduced, M2 macrophage/total macrophage ratios in the wound area in rMFG-E8-treated mice were not different from those in control mice, suggesting that rMFG-E8 might suppress the number of total macrophages, especially M1 macrophages, which infiltrated into the wounded area.

rMFG-E8 suppressed apoptotic cells after cutaneous I/R

I/R-induced reactive oxygen species causes apoptosis and subsequent exaggerated inflammatory responses induced by secondary necrosis (Miksa *et al.*, 2009; Aziz *et al.*, 2011). To examine the influence of MFG-E8 on the number of apoptotic cells in I/R areas, TUNEL staining of skin sections was performed. At 1 day after reperfusion, the number of apoptotic cells in I/R areas in rMFG-E8-treated mice were decreased compared with those in control mice (Figure 4). These results suggest that rMFG-E8 might suppress the formation and/or accumulation of apoptotic cells induced by cutaneous I/R injury.

rMFG-E8 suppressed the production of proinflammatory cytokines and chemokines after cutaneous I/R

Next we investigated the effect of MFG-E8 on the mRNA levels of proinflammatory cytokines and chemokines, including MCP-1, IL-1β, TNF-α, and IL-6, in the I/R area by real-time PCR. Treatment with rMFG-E8 significantly suppressed mRNA levels of proinflammatory cytokines and chemokines (Figure 5a–d). These results suggest that rMFG-E8 might suppress the inflammation of skin after I/R.

Next we examined the production of intracellular inflammatory cytokines and chemokines in infiltrating macrophages in the I/R sites using fluorescence-activated cell sorting analysis, because macrophages, rather than neutrophils, are major sources of proinflammatory cytokines and chemokines, including IL-6, TNF-α, and MCP-1. Similar to the results of histological analyses depicted in Figure 3, the total number of infiltrating $CD68^+$ macrophages in I/R sites was inhibited by rMFG-E8 treatment (Figure 5e). The ratios of MCP-1^+ macrophages/total macrophages, TNF-α^+ macrophages/total macrophages, and IL-6^+ macrophages/total macrophages in I/R sites were also inhibited by rMFG-E8 treatment (Figure 5f–h). These results suggest that rMFG-E8 might inhibit the recruitment of macrophages, as well as the production of proinflammatory cytokines and chemokines, in macrophages.

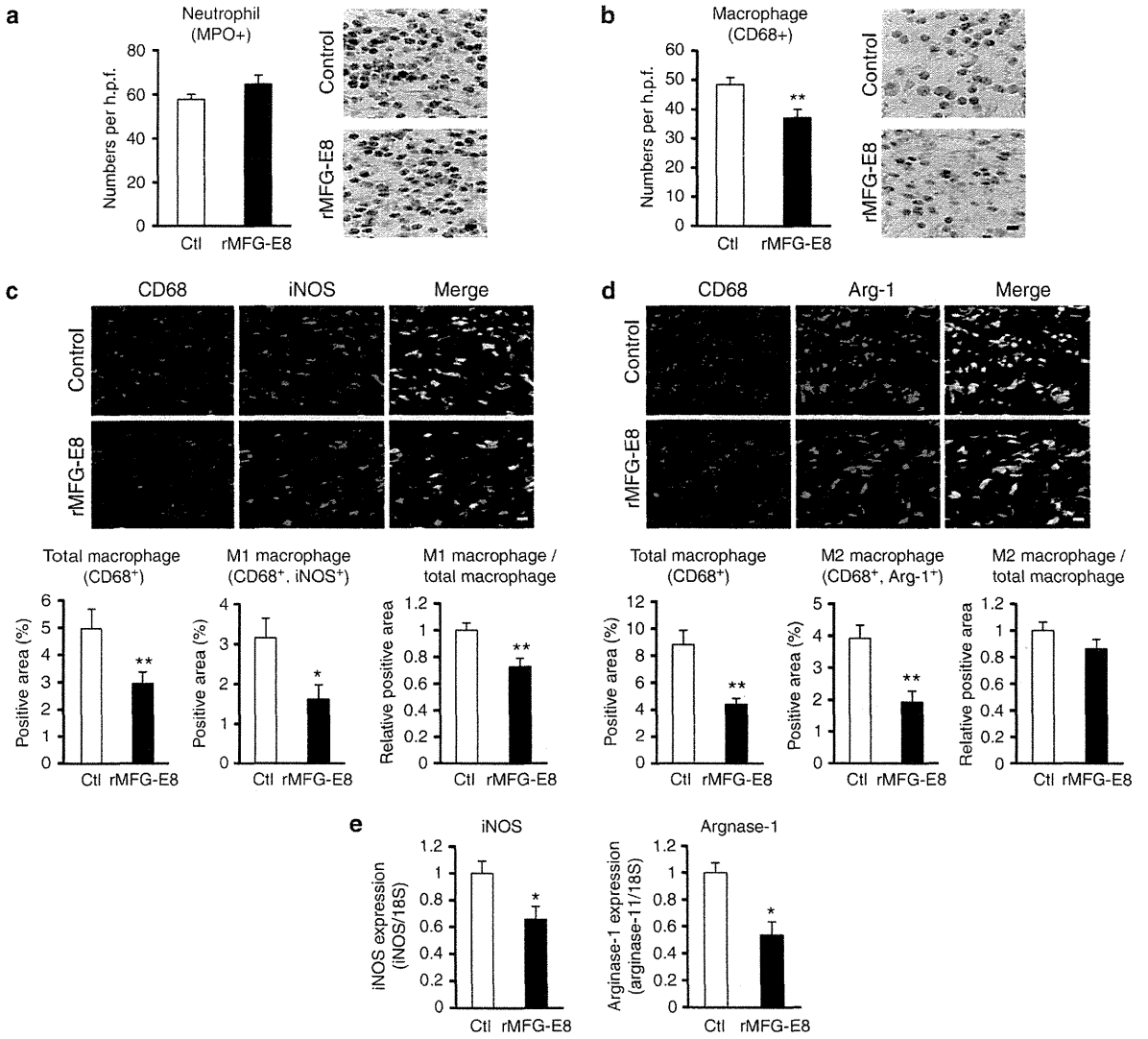

Figure 3. rMFG-E8 suppressed infiltrating macrophages, especially M1 macrophages, into the cutaneous ischemia–reperfusion (I/R) area. (**a**) The number of infiltrating neutrophils in the I/R site at 1 day after reperfusion was determined by counting myeloperoxidase-positive cells. Values were determined in six random microscopic fields in $n=3$ mice per groups. Scale bar = 20 μm. (**b**) The number of infiltrating macrophages in the I/R site at 1 day after reperfusion was determined by counting CD68-positive cells. Values were determined in six random microscopic fields in $n=3$ mice per group. $^{**}P<0.01$. Scale bar = 20 μm. (**c**, **d**) Infiltration of $CD68^+$ and induced nitric oxide synthase (iNOS)$^+$ M1 macrophages (**c**) or $CD68^+$ and arginase-1^+ M2 macrophage (**d**) in the I/R area 1 day after reperfusion. Quantification of the $CD68^+$, $iNOS^+$, and arginase-1^+ areas in six random microscopic fields in $n=3$ mice per group was performed using the Image J software. The ratio of M1 or M2 macrophages (M1 or M2 macrophages/Total macrophages) in control mice was assigned a value of 1. $^{**}P<0.01$, $^{*}P<0.05$. Scale bar = 20 μm. (**e**) Quantification of iNOS and arginase-1 mRNA levels in I/R area at 1 day after reperfusion. $n=3$ mice per group. $^{*}P<0.05$.

rMFG-E8 promoted angiogenesis in the I/R area after cutaneous I/R

We previously determined that blood vessel formation was inhibited in cutaneous wound area in MFG-E8 KO mice, suggesting that MFG-E8 might regulate angiogenesis in cutaneous wound healing. Therefore, we investigated the effect of rMFG-E8 on vascularity in the I/R area. At 6 days after reperfusion, the numbers of $CD31^+$ ECs and $NG2^+$ pericytes in the I/R areas were significantly increased compared with those in control mice (Figure 6a). The numbers of αSMA^+ (α-smooth muscle actin) pericytes/vascular SMCs in I/R areas in rMFG-E8-treated mice tended to be more than those in control mice (Figure 6b). These results suggest that rMFG-E8 might enhance angiogenesis in I/R injury.

The effects of rMFG-E8 on IFA-induced skin inflammation

To examine whether the effects of rMFG-E8 are specific to I/R injury or globally relate to skin inflammation, we next analyzed the effect of MFG-E8 on the skin inflammation induced by incomplete Freund's adjuvant (IFA). It has been known that IFA injection into the skin induced skin inflammatory response, such as inflammatory cells infiltration and

proinflammatory cytokines production (Vitoriano-Souza *et al.*, 2012). IFA-injected sites were treated with subcutaneous injection of rMFG-E8 or phosphate-buffered saline as a control. The appearance of skin at 1 day after IFA injection did not differ between the two groups (Supplementary Figure S1a online). rMFG-E8 treatment did not affect the number of neutrophils, total macrophages, and M1 macrophages in the IFA-injected site at 1 day after IFA injection (Supplementary Figure S1b,c online). No significant difference in the number of apoptotic cells was observed between the two groups (Supplementary Figure S1e online). mRNA levels of iNOS, arginase-1, MCP-1, IL-1β, TNF-α, and IL-6 in IFA-injected skin in rMFG-E8-treated mice were also comparable to those in control mice at 1 day after IFA injection (Supplementary Figure S1d and S2 online). These results indicate that rMFG-E8 did not modify IFA-induced skin inflammation.

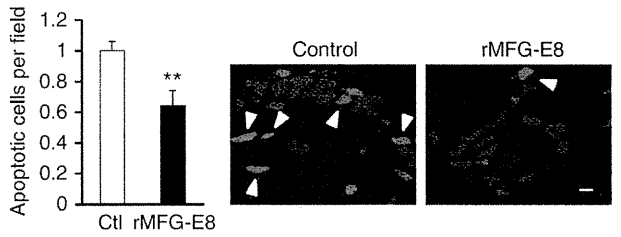

Figure 4. rMFG-E8 suppressed apoptotic cells after cutaneous ischemia–reperfusion (I/R). The number of apoptotic cells in the I/R site at 1 day after reperfusion was determined by counting both TUNEL- and DAPI (4′,6-diamidino-2-phenylindole)-positive cells (Arrowhead). Values were determined in 6 random microscopic fields in $n = 3$ mice per group. $^{**}P < 0.01$. Scale bar = 20 μm.

DISCUSSION

This is a study to investigate the role of MFG-E8 in cutaneous I/R injury. Using murine model (Stadler *et al.*, 2004), we determined that MFG-E8 expression was significantly increased in the skin during ischemia, suggesting that MFG-E8 expression might be enhanced by hypoxic conditions. Immunofluorescence staining of MFG-E8 revealed that MFG-E8 expression levels around ECs and pericytes/vascular SMCs just after reperfusion (0 hour) were enhanced compared with those before ischemia (−12 hours) and at 72 hours after reperfusion (72 hours), suggesting that ECs and pericytes/vascular SMCs might be primary sources of MFG-E8 during ischemia. In addition, we confirmed that mRNA and/or protein levels of MFG-E8 in pericytes and ECs were significantly enhanced by hypoxia in a time-dependent manner. These findings suggest that hypoxia in ischemic areas might be associated with the enhancement of MFG-E8 expression in pericytes/vascular SMCs and ECs. Previous studies have reported that MFG-E8 mRNA and protein expression in organs, including the kidney, liver, and gut, were significantly decreased by I/R (Matsuda *et al.*, 2011; Wu *et al.*, 2012; Deroide *et al.*, 2013; Matsuda *et al.*, 2013). Consistent with these previous results, MFG-E8 expression in cutaneous I/R areas was decreased by 0.5-fold at 72 hours after reperfusion. The pathogenesis of the suppression of MFG-E8 expression after I/R is currently unknown; however, we suggest that I/R might cause severe damage of tissue, including pericytes/vascular SMCs and ECs, and this I/R-induced damage to the source of MFG-E8 may account for the suppression of MFG-E8 expression after I/R. Kasuya *et al.*(2014) reported that blood vessels in the I/R areas were reduced compared with those in marginal zones after

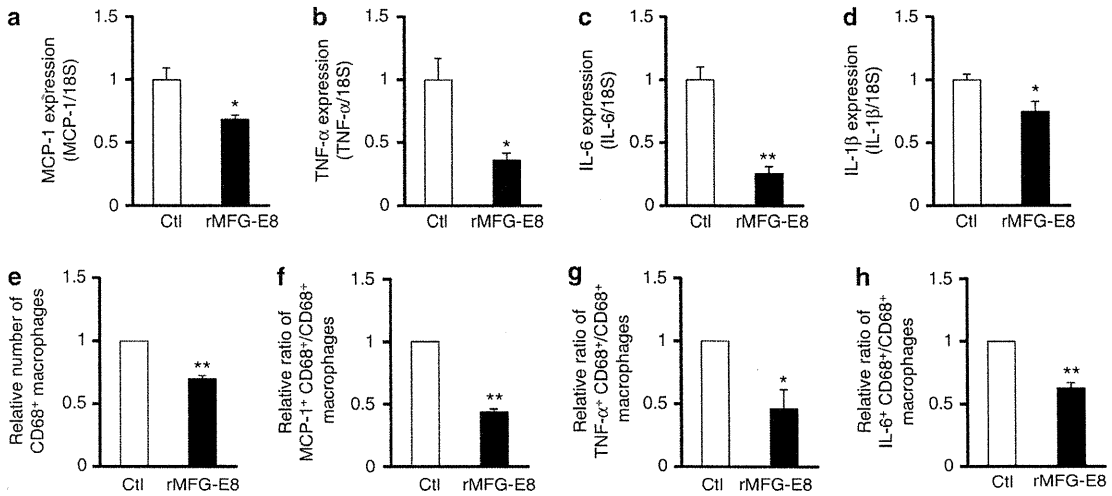

Figure 5. rMFG-E8 suppressed the production of proinflammatory cytokines after cutaneous ischemia–reperfusion (I/R). Quantification of mRNA levels of monocyte chemotactic protein-1 (MCP-1) (**a**), IL-1β (**b**), tumor necrosis factor α (TNF-α) (**c**), and IL-6 (**d**) in the I/R area at 1 day after reperfusion by quantitative reverse transcriptase–PCR (RT–PCR). mRNA levels in control mice were assigned values of 1. (**e–h**) Flow cytometry analyses of the production of intracellular inflammatory cytokines and chemokines in infiltrated macrophages in the I/R site. (**e**) The relative number of infiltrated CD68 + macrophages in the I/R site. Total number of macrophages in control mice was assigned a value of 1. (**f**) The relative ratio of MCP-1 + macrophages/total macrophages, (**g**) TNF-α$^+$ macrophages/total macrophages, and (**h**) IL-6$^-$ macrophages/total macrophages in the I/R site. The ratio of MCP-1$^-$, TNF-α$^+$, or IL-6$^-$ macrophages/total macrophages in control mice was assigned a value of 1. $n = 3$ mice per group. $^{**}P < 0.01$, $^{*}P < 0.05$.

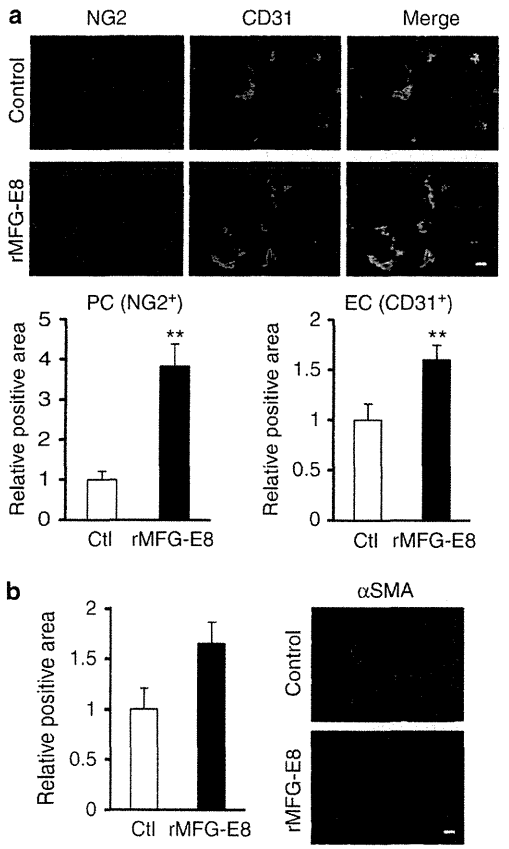

Figure 6. rMFG-E8 promoted angiogenesis in the ischemia–reperfusion (I/R) area after cutaneous I/R. (**a**) The amount of $CD31^+$ ECs and $NG2^+$ pericytes in the cutaneous I/R area at 6 days after reperfusion. (**b**) The amount of α-smooth muscle actin (αSMA^+) myofibroblast or pericytes in the cutaneous I/R area at 6 days after reperfusion. Quantification of the $CD31^+$, $NG2^+$, and αSMA^+ areas in 6 random microscopic fields in $n=3$ mice per group was performed using the Image J software. Positive area in control mice was assigned a value of 1. $^{**}P<0.01$, $^{*}P<0.05$.

reperfusion, suggesting that I/R-induced reactive oxygen species might damage the blood vessels (Kasuya *et al.*, 2014).

We determined that the injection of rMFG-E8 significantly inhibited the formation of ulcers after I/R; however, the differences of the formation of ulcers after I/R between MFG-E8 WT and KO mice were not strikingly different. The reason why the KO mice have not had a more marked response is unknown. However, we suggest that the immediate suppression of MFG-E8 expression in the I/R site after I/R in WT mice may lead to no remarkable difference of MFG-E8 expression in the I/R site after I/R between WT and KO mice.

We identified rMFG-E8-mediated protective mechanisms of cutaneous I/R injury, including (i) suppression of macrophages, especially M1 macrophages, infiltrating into the I/R area; (ii) suppression of apoptotic cell accumulation; (iii) suppression of proinflammatory cytokine synthesis; and (iv) enhancement of angiogenesis. We recently demonstrated that MFG-E8 regulates angiogenesis and wound healing in a cutaneous wound healing mice model (Uchiyama *et al.*, 2014). In the present study using a murine I/R model, we additionally determined that MFG-E8 regulates the functions of M1 macrophages, including the secretion of proinflammatory cytokines.

M1 macrophages infiltrate in the early phase of response to tissue damage, and they are involved in cutaneous injury and inflammation by secreting proinflammatory mediators, including MCP-1, NO, IL-1, IL-6, IL-12, and TNF-α (Mosser, 2003; Saito *et al.*, 2008; Lawrence and Natoli, 2011). Therefore, our results indicate that MFG-E8 suppresses the M1 macrophage infiltration, through which cutaneous inflammation induced by proinflammatory mediators from M1 macrophages is restrained. With respect to M1 macrophages and MFG-E8, it has been reported that coculture of macrophages with apoptotic prostate cancer cells increased efferocytosis, elevated MFG-E8 expression levels, and induced macrophage polarization into the M2 phenotype (Soki *et al.*, 2014). They also demonstrated that MFG-E8 enhanced the phosphorylation of STAT3, and inhibited SOCS3, a negative regulator of STAT3, therefore keeping STAT3 signaling activated and promoting M2 polarization. This study suggests that rMFG-E8 might induce M2 macrophage polarization in the I/R area, resulting in the suppression of M1 macrophage ratios. However, M2 macrophage ratios were not increased by rMFG-E8 treatment in our experiments. Therefore, further studies are required to clarify the effect of MFG-E8 on M1/M2 macrophages.

It has been well recognized that MFG-E8 acts as a bridging protein between phosphatidylserine on apoptotic cells and integrin αvβ3/5 on phagocytes, thereby enhancing phagocytosis and clearance of apoptotic cells (Hanayama *et al.*, 2002; Asano *et al.*, 2004). In an experimental sepsis model using cecal ligation and puncture, MFG-E8-containing exosome administration attenuated the acute systemic inflammatory response in sepsis by enhancing apoptotic cell clearance (Miksa *et al.*, 2009). We showed that treatment with rMFG-E8 decreased I/R-induced apoptotic cell accumulation. These findings suggest that the decreased levels of MFG-E8 after cutaneous I/R may be associated with impaired phagocytosis, leading to the accumulation of apoptotic cells in the I/R area, and that the administration of rMFG-E8 may enhance phagocytosis of apoptotic cells, leading to the suppression of apoptosis and necrosis in the I/R area and protection from pressure ulcers.

We assessed vascularity in I/R areas, and found that the numbers of ECs and pericytes in the I/R areas were significantly more than those in control mice. We assume that the protective effect of rMFG-E8 on cutaneous I/R injury might be associated with both suppression of inflammation and promotion of angiogenesis.

Finally, we demonstraed that rMFG-E8 did not affect IFA-induced skin inflammation, suggesting that the inhibition of skin inflammation by rMFG-E8 treatment may be relatively restricted in cutaneous I/R injury. However, further investigation may be warranted in additional skin inflammation models.

Taken together, we conclude that MFG-E8 suppresses the formation of pressure ulcers induced by cutaneous I/R injury by regulating inflammation and angiogenesis. Exogenous MFG-E8 administration has possible therapeutic potential for

cutaneous I/R injuries, including decubitus ulcers and Raynaud's phenomenon–induced digital ulcers.

MATERIALS AND METHODS

The detailed protocols and statistical analysis are described in Supplementary Materials and Methods online.

Mice

C57BL/6 mice were purchased from the SLC (Shizuoka, Japan). 8- to 12-week-old mice were used for all experiments. MFG-E8 KO C57BL/6 mice were generated as previously described (Neutzner *et al.*, 2007; Motegi *et al.*, 2011a). All experiments were approved by the Ethical Committee for Animal Experiments of the Gunma University Graduate School of Medicine and carried out in accordance with the approved guidelines.

I/R cycles and analysis

The I/R model that has been previously reported was used (Peirce *et al.*, 2000; Stadler *et al.*, 2004; Saito *et al.*, 2008). The dorsal skin was gently pulled up and trapped between two round ferrite magnetic plates that had a 12-mm diameter (113 mm^2) and that were 5-mm thick (NeoMag Co, Ichikawa, Japan) for 12 hours, and then plates were removed. All of the mice developed two round ulcers separated by a bridge of normal skin. For analysis, each wound site was digitally photographed after wounding, and the wound areas were measured on photographs using Image J (version 1.48, NIH, Bethesda, MD). To assess the effects of rMFG-E8 on wound healing after cutaneous I/R injury, 400 ng of rMFG-E8 (R&D systems, Minneapolis, MN) per 50 μl of phosphate-buffered saline or 50 μl of phosphate-buffered saline as a control were injected into the dermis in the I/R site at the beginning of reperfusion.

Real-time RT–PCR

To analyze the mRNA levels of expression in the I/R site by real-time RT–PCR, the whole-skin samples in the I/R site were used. Real-time RT–PCR was performed as described in Supplementary Materials and Methods online.

Statistics

P-values were calculated using the Student's *t*-test (two-sided) or by analysis of one-way analysis of variance followed by Bonferroni's post test, as appropriate. Error bars represent s.e.m., and numbers of experiments (*n*) are as indicated.

CONFLICT OF INTEREST

The authors state no conflict of interest.

ACKNOWLEDGMENTS

This work was supported by a Grant from the Adaptable and Seamless Technology transfer Program (A-STEP), Japan Science and Technology Agency.

SUPPLEMENTARY MATERIAL

Supplementary material is linked to the online version of the paper at http://www.nature.com/jid

REFERENCES

Andersen MH, Berglund L, Rasmussen JT *et al.* (1997) Bovine PAS-6/7 binds alpha v beta 5 integrins and anionic phospholipids through two domains. *Biochemistry* 36:5441–6

Asano K, Miwa M, Miwa K *et al.* (2004) Masking of phosphatidylserine inhibits apoptotic cell engulfment and induces autoantibody production in mice. *J Exp Med* 200:459–67

Aziz M, Jacob A, Matsuda A *et al.* (2011) Review: milk fat globule-EGF factor 8 expression, function and plausible signal transduction in resolving inflammation. *Apoptosis* 16:1077–86

Carden DL, Granger DN (2000) Pathophysiology of ischaemia-reperfusion injury. *J Pathol* 190:255–66

Carmo-Araújo EM, Dal-Pai-Silva M, Dal-Pai V *et al.* (2007) Ischaemia and reperfusion effects on skeletal muscle tissue: morphological and histochemical studies. *Int J Exp Pathol* 88:147–54

Deroide N, Li X, Lerouet D *et al.* (2013) MFGE8 inhibits inflammasome-induced IL-1β production and limits postischemic cerebral injury. *J Clin Invest* 123:1176–81

Ferrante CJ, Leibovich SJ (2011) Regulation of Macrophage Polarization and Wound. *Adv Wound Care (New Rochelle)* 1:10–6

Gorecki C, Brown JM, Nelson EA *et al.* (2009) Impact of pressure ulcers on quality of life in older patients: a systematic review. *J AM Geriatr Soc* 67:1175–83

Hanayama R, Tanaka M, Miwa K *et al.* (2002) Identification of a factor that links apoptotic cells to phagocytes. *Nature* 417:182–7

Kasuya A, Sakabe J, Tokura Y (2014) Potential application of in vivo imaging of impaired lymphatic duct to evaluate the severity of pressure ulcer in mouse model. *Sci Rep* 4:4173

Lawrence T, Natoli G (2011) Transcriptional regulation of macrophage polarization: enabling diversity with identity. *Nat Rev Immunol* 11:750–61

Matsuda A, Jacob A, Wu R *et al.* (2013) Milk fat globule–EGF factor VIII ameliorates liver injury after hepatic ischemia-reperfusion. *J Surg Res* 180:e37–46

Matsuda A, Wu R, Jacob A *et al.* (2011) Protective effect of milk fat globule-epidermal growth factor-factor VIII after renal ischemia-reperfusion injury in mice. *Crit Care Med* 39:2039–47

Miksa M, Wu R, Dong W *et al.* (2009) Immature dendritic cell-derived exosomes rescue septic animals via milk fat globule epidermal growth factor-factor VIII. *J Immunol* 183:5983–90

Mosser DM (2003) The many faces of macrophage activation. *J Leukoc Biol* 73:209–12

Motegi S, Garfield S, Feng X *et al.* (2011b) Potentiation of platelet-derived growth factor receptor-β signaling mediated by integrin-associated MFG-E8. *Arterioscler Thromb Vasc Biol* 31:2653–64

Motegi S, Leitner WW, Lu M *et al.* (2011a) Pericyte-Derived MFG-E8 Regulates Pathologic Angiogenesis. *Arterioscler Thromb Vasc Biol* 31:2024–34

Nathan C, Xie QW (1994) Nitric oxide synthases: roles, tolls, and controls. *Cell* 78:915–8

Neutzner M, Lopez T, Feng X *et al.* (2007) MFG-E8/Lactadherin Promotes Tumor Growth in an Angiogenesis-Dependent Transgenic Mouse Model of Multistage Carcinogenesis. *Cancer Res* 67:6777–85

Ogura K, Nara K, Watanabe Y *et al.* (1993) Cloning and expression of cDNA for O-acetylation of GD3 ganglioside. *Biochem Biophys Res Commun* 225:932–8

Peirce SM, Skalak TC, Rodeheaver GT (2000) Ischemia-reperfusion injury in chronic pressure ulcer formation: a skin model in the rat. *Wound Repair Regen* 8:68–76

Pretto EA Jr (1991) Reperfusion injury of the liver. *Transplant Proc* 23:1912–4

Reid RR, Sull AC, Mogford JE *et al.* (2004) A novel murine model of cyclical cutaneous ischemia-reperfusion injury. *J Surg Res* 116:172–80

Saito Y, Hasegawa M, Fujimoto M *et al.* (2008) The loss of MCP-1 attenuates cutaneous ischemia-reperfusion injury in a mouse model of pressure ulcer. *J Invest Dermatol* 128:1838–51

Salcido R, Donofrio JC, Fisher SB *et al.* (1994) Histopathology of pressure ulcers as a result of sequential computer-controlled pressure sessions in a fuzzy rat model. *Adv Wound Care* 7:23–4

Silvestre JS, Théry C, Hamard G *et al.* (2005) Lactadherin promotes VEGF-dependent neovascularization. *Nat Med* 11:499–506

Soki FN, Koh AJ, Jones JD *et al.* (2014) polarization of prostate cancer associated macrophages is induced by milk-fat globule-

EGF factor 8 (MFG-E8) mediated efferocytosis. *J Biol Chem* 289: 24560–72

Stadler I, Zhang RY, Oskoui P *et al.* (2004) Development of a simple, noninvasive, clinically relevant model of pressure ulcers in the mouse. *J Invest Surg* 17:221–7

Stubbs JD, Lekutis C, Singer KL *et al.* (1990) cDNA cloning of a mouse mammary epithelial cell surface protein reveals the existence of epidermal growth factor-like domains linked to factor VIII-like sequences. *Proc Natl Acad Sci USA* 87:8417–21

Taylor MR, Couto JR, Scallan CD *et al.* (1997) Lactadherin (formerly BA46), a membrane-associated glycoprotein expressed in human milk and breast carcinomas, promotes Arg-Gly-Asp (RGD)-dependent cell adhesion. *DNA Cell Biol* 16:861–9

Uchiyama A, Yamada K, Ogino S *et al.* (2014) MFG-E8 regulates angiogenesis in cutaneous wound healing. *Am J Pathol* 184: 1981–90

Vitoriano-Souza J, Moreira Nd, Teixeira-Carvalho A *et al.* (2012) Cell recruitment and cytokines in skin mice sensitized with the vaccine adjuvants: saponin, incomplete Freund's adjuvant, and monophosphoryl lipid A. *PLoS One* 7:e40745

Woolfson RG, Millar CG, Neild GH (1994) Ischaemia and reperfusion injury in the kidney: current status and future direction. *Nephrol Dial Transplant* 9:1529–31

Wu R, Dong W, Wang Z *et al.* (2012) Enhancing apoptotic cell clearance mitigates bacterial translocation and promotes tissue repair after gut ischemia-reperfusion injury. *Int J Mol Med* 30:593–8

JAPANESE DERMATOLOGICAL ASSOCIATION
THE JOURNAL OF DERMATOLOGY
doi: 10.1111/1346-8138.12775
Journal of Dermatology 2015; **42**: 283–287

ORIGINAL ARTICLE

Clinical and laboratory features of systemic sclerosis complicated with localized scleroderma

Sayaka TOKI, Sei-ichiro MOTEGI, Kazuya YAMADA, Akihiko UCHIYAMA, Sahori KANAI, Masayoshi YAMANAKA, Osamu ISHIKAWA

Department of Dermatology, Gunma University Graduate School of Medicine, Maebashi, Japan

ABSTRACT

Localized scleroderma (LSc) primarily affects skin, whereas systemic sclerosis (SSc) affects skin and various internal organs. LSc and SSc are considered to be basically different diseases, and there is no transition between them. However, LSc and SSc have several common characteristics, including endothelial cell dysfunction, immune activation, and excess fibrosis of the skin, and there exist several SSc cases complicated with LSc during the course of SSc. Clinical and laboratory characteristics of SSc patients with LSc remain unclear. We investigated the clinical and laboratory features of 8 SSc patients with LSc among 220 SSc patients (3.6%). The types of LSc included plaque (5/8), guttate (2/8), and linear type (1/8). All cases were diagnosed as having SSc within 5 years before or after the appearance of LSc. In three cases of SSc with LSc (37.5%), LSc skin lesions preceded clinical symptoms of SSc. Young age, negative antinuclear antibody, and positive anti-RNA polymerase III antibody were significantly prevalent in SSc patients with LSc. The positivity of anticentromere antibody tended to be prevalent in SSc patients without LSc. No significant difference in the frequency of complications, such as interstitial lung disease, reflux esophagitis, and pulmonary artery hypertension, was observed. The awareness of these characteristic of SSc with LSc are essential to establish an early diagnosis and treatment.

Key words: localized scleroderma, morphea, systemic sclerosis.

INTRODUCTION

Systemic scleroderma (SSc) is a generalized disease characterized by fibrosis of the skin and internal organs, vascular dysfunction, and immune disorder.[1–4] Localized scleroderma (LSc) is a disease with sclerotic lesions (fibrosis) of the skin and underneath the skin. It is generally differentiated from SSc by the lack of Raynaud's phenomenon and visceral involvements. Although the prognosis of LSc is generally favorable, it occasionally reveals serological and growth abnormalities, as well as deformation and motor dysfunction of the extremities.[5] LSc and SSc have several common characteristics including endothelial cell dysfunction, Th2-dominant immune activation, and excess fibrosis of the skin with similar pathological findings.[6–10] Previous studies have shown that 4.9–6.7% of SSc cases are complicated with LSc.[11–13] However, the demographic and clinical features of these patients have not been well characterized. In this study, we clinically investigated the patients with SSc complicated with LSc.

METHODS

Patients

We analyzed 220 Japanese patients with SSc who visited Gunma University Hospital from 2006 to 2013. All patients fulfilled the criteria of SSc proposed by the American College of Rheumatology.[14] Patients were classified into limited cutaneous type and diffuse cutaneous type of SSc according to the classification by LeRoy *et al.*[15]

LSc was diagnosed from its characteristic clinical finding of glossy, well-defined local sclerotic lesions along with the histological findings of sclerotic lesions. The disease types of LSc are largely classified into plaque type, linear type, and generalized morphea, along with subtypes including guttate type, bullous type, and deep type.[16] Generalized morphea was defined as four or more LSc lesions with a diameter of 3 cm or greater in two or more anatomical sites.[17] This study was approved by the local research ethics committee of Gunma University. Patients provided written informed consent before participation.

Clinical and laboratory assessments

Skin sclerosis was measured by the modified Rodnan total skin score. Interstitial lung disease was detected as bibasilar interstitial fibrosis or a ground-glass shadow visible on high-resolution computed tomography scans. Pulmonary artery hypertension was defined as an elevated right ventricular systolic pressure (>45 mmHg) on echocardiography and, subsequently, as an elevated mean pulmonary artery pressure (>25 mmHg) during cardiac catheterization. Reflux esophagitis

Correspondence: Sei-ichiro Motegi, M.D., Ph.D., Department of Dermatology, Gunma University Graduate School of Medicine, 3-39-22 Showa, Maebashi, Gunma 371-8511, Japan. Email: jsmotegi@gunma-u.ac.jp
Received 30 October 2014; accepted 9 December 2014.

Table 1. Summary of nine patients of SSc with LSc

Case	Onset age of SSc with LSc (years)	Sex	RP	SD	DPS	SSc type	Autoantibody	Complication			LSc		Duration between LSc and SSc	Past history	ACR/EULAR criteria score
								ILD	RE	PAH	Type	Location			
1	44	F	–	+	–	lcSSc	RNAP	+	–	–	Plaque	Chest, abdomen, lower back	10 months (LSc→SSc)	–	12
2	37	F	–	+	–	lcSSC	Centromere	–	–	–	Guttate	Buttock, thigh	4 years (LSc→SSc)	AD	10
3	28	M	+	+	–	dcSSc	RNAP	–	–	–	Plaque (GM)	Face, chest, abdomen, upper arm, lower extremity	5 years (LSc→SSc)	AD, asthma	19
4	44	M	+	+	–	dcSSc	Topo I	+	+	–	Guttate	Face, chest, abdomen, back, thigh	1 year (SSc→LSc)	–	28
5	61	F	+	+	–	dcSSc	–	+	+	–	Plaque (GM)	Chest, abdomen, lower leg	1 year (SSc→LSc)	–	20
6	57	F	+	+	–	lcSSc	Topo I	–	+	–	Plaque	Chest	1.5 years (SSc→LSc)	Hashimoto's disease	19
7	54	F	+	+	+	dcSSc	–	+	+	–	Plaque (GM)	Chest, abdomen, back, upper arm, thigh	2 years (SSc→LSc)	–	21
8	37	F	+	+	–	lcSSC	Topo I, RNP	–	–	–	Linear	Chest	4 years (SSc→LSc)	–	12

ACR/EULAR, American College of Rheumatology/European League Against Rheumatism; AD, atopic dermatitis; ANA, antinuclear antibody; centromere, anticentromere antibody; dcSSc, diffuse cutaneous type of SSc; DPS, digital pitting scars; GM, generalized morphea; ILD, interstitial lung disease; lcSSc, limited cutaneous type of SSc; LSc, localized scleroderma; PAH, pulmonary artery hypertension; RA, rheumatoid arthritis; RE, reflux esophagitis; RNAP, anti-RNA polymerase III antibody; RNP, ribonucleoprotein; RP, Raynaud's phenomenon; SD, sclerodactyly; SSc, systemic scleroderma; Topo I, anti-topoisomerase I antibody. Patients with a total score ≥9 according to the ACR/EULAR classification were classified as having definite SSc.